387

Wolfsberg et al.

LA-9225-PR

Progress Report

Los Alamos National Laboratory is operated by the University of California for the United States Department of Energy under contract W-7405-ENG-36.

Research and Development Related to the Nevada Nuclear Waste Storage Investigations

October 1—December 31, 1981

Los Alamos

Los Alamos National Laboratory
Los Alamos, New Mexico 87545

The four most recent reports in this series, unclassified, are LA-8739-PR, LA-8847-PR, LA-8959-PR, and LA-9095-PR.

This report was prepared by the Los Alamos National Laboratory as part of the Nevada Nuclear Waste Storage Investigations managed by the Nevada Operations Office of the US Department of Energy. Based upon their applicability to the investigations, some results for the Radionuclide Migration Project, managed by the Nevada Operations Office of the US Department of Energy, are included in this report.

LA-9225-PR
Progress Report

UC-70
Issued: April 1982

Research and Development Related to the Nevada Nuclear Waste Storage Investigations

October 1—December 31, 1981

Compiled and Edited by

K. Wolfsberg
W. R. Daniels
D. T. Vaniman
B. R. Erdal

Contributors

R. D. Aguilar
R. Anderson
B. Arney
W. S. Baldridge
B. P. Bayhurst
G. E. Bentley
D. L. Bish
J. D. Blacic
D. Broxton
P. L. Bussolini
F. A. Caporuscio
J. Carter
M. R. Cisneros
B. M. Crowe
W. R. Daniels
C. J. Duffy
B. R. Erdal
R. R. Geoffrion
R. D. Golding*
R. C. Gooley
P. M. Halleck
G. H. Heiken
P. Johnson
J. F. Kerrisk
S. D. Knight
F. O. Lawrence
S. Maestas
P. L. McGuire
T. J. Merson
A. J. Mitchell
C. W. Myers
D. C. Nelson
J. W. Neudecker
T. W. Newton
A. E. Ogard
P. Q. Oliver
F. V. Perry
N. A. Raybold
R. J. Romero
R. S. Rundberg
V. L. Rundberg
R. E. Semarge
T. J. Shankland
W. L. Sibbitt
J. J. Simpson
K. C. Spicochi
G. M. Thompson*
J. L. Thompson**
E. N. Treher
D. T. Vaniman
G. R. Walter*
P. L. Wanek
K. Wolfsberg

*Department of Hydrology and Water Resources, University of Arizona, Tucson, AZ 85721.
**Department of Chemistry, Idaho State University, Pocatello, ID 83209.

Los Alamos
Los Alamos National Laboratory
Los Alamos, New Mexico 87545

RESEARCH AND DEVELOPMENT RELATED TO THE NEVADA NUCLEAR WASTE STORAGE INVESTIGATIONS

October 1 - December 31, 1981

Compiled and Edited by

K. Wolfsberg, W. R. Daniels, D. T. Vaniman, and B. R. Erdal

Contributors

R. D. Aguilar
R. Anderson
B. Arney
W. S. Baldridge
B. P. Bayhurst
G. E. Bentley
D. L. Bish
J. D. Blacic
D. Broxton
P. L. Bussolini
F. A. Caporuscio
J. Carter
M. R. Cisneros
B. M. Crowe
W. R. Daniels
C. J. Duffy
B. R. Erdal
R. R. Geoffrion
R. D. Golding*
R. C. Gooley
P. M. Halleck
G. H. Heiken
P. Johnson
J. F. Kerrisk
S. D. Knight
F. O. Lawrence
S. Maestas
P. L. McGuire
T. J. Merson
A. J. Mitchell
C. W. Myers
D. C. Nelson
J. W. Neudecker
T. W. Newton
A. E. Ogard
P. Q. Oliver
F. V. Perry
N. A. Raybold
R. J. Romero
R. S. Rundberg
V. L. Rundberg
R. E. Semarge
T. J. Shankland
W. L. Sibbitt
J. J. Simpson
K. C. Spicochi
G. M. Thompson*
J. L. Thompson**
E. N. Treher
D. T. Vaniman
G. R. Walter*
P. L. Wanek
K. Wolfsberg

ABSTRACT

This report summarizes the contribution of the Los Alamos National Laboratory to the Nevada Nuclear Waste Storage Investigations for the first quarter of FY-1982.

I. INTRODUCTION

This report summarizes some of the technical contributions from the Los Alamos National Laboratory to the Nevada Nuclear Waste Storage Investigations (NNWSI) project managed by the Nevada Operations Office of the US Department of Energy during the period from October 1 through December 31, 1981. This report is not intended to be a detailed technical document but does indicate the status of some of the investigations being performed at Los Alamos.

II. WASTE PACKAGE DEVELOPMENT

Sorption of Anions on Possible Backfill Components (E. N. Treher and N. A. Raybold)

The results of the sorption of technetium on graphite are given in Table I with the R_d values for sorption of I^- for comparison. There was essentially no change in pH during the experiment.

III. FIELD MIGRATION EXPERIMENTS - RELATED LABORATORY STUDIES

A. Preparation of Rock-Treated Water (A. J. Mitchell, P. L. Wanek, K. Wolfsberg, and G. E. Bentley)

The experiment for preparing 200 ℓ of G-Tunnel rock-treated water[1] was essentially completed after the water from well J-13 had been contacted with muck from G Tunnel for 28 days, filtered, contacted with fresh muck for 24 days,

TABLE I

SORPTION OF TECHNETIUM AND IODINE ON GRAPHITE

	R_d (mℓ/g)		
Contact Time (days)	I	Tc	Final pH[a]
1	0.9	1.1	8.65
7	1.7	2.5	8.57
21	2.5	1.6	8.69
42	11	0.6	8.67
63	32	---	8.49

[a]The pH of the initial solutions was 8.67.

and filtered again. Final membranes in both filtrations were 0.05-μm Nuclepore polycarbonate filters. Aliquots of the water were removed at frequent intervals during the contacts and filtered through 0.05-μm Nuclepore membranes. A portion of each aliquot was acidified for determination of cations and silicon by emission spectroscopy. Concentrations of anions were determined by ion chromatography on nonacidified samples. The results of these analyses are given in Tables II and III; the composition of water from well J-13 is given for comparison in each table.

The average experimental normalities of the rock-treated water are 3.17 meq/ℓ for cations and 2.68 meq/ℓ for anions. The average values for well J-13 water are 2.85 meq/ℓ for cations and 3.22 meq/ℓ for anions. The differences of normalities for cations and anions of 18% and 12% for these two waters are slightly higher than differences of 1% to 15% typically observed by the US Geological Survey in water analyses (see, for example, Ref. 2). Part of the differences in normalities of anions and cations may be due to loss of CO_2, and therefore HCO_3^-, from the solutions. This possibility is being investigated by determination of alkalinity by titration with acid. For groundwaters, such as that from well J-13, in the range of pH 8 to 9, the principal component of alkalinity should be HCO_3^- because basic constituents such as phosphate have not been detected.

The pH of the water varied <0.08 unit during preparation of the rock-treated water. The average value is 8.32 ± 0.03.

B. Development and Characterization of Water Tracers (P. L. Wanek and K. Wolfsberg)

We are developing methods for separation and identification of potential groundwater tracers. Initial work with water tracers and the basic means for their separation was done at the University of Arizona.[1] A class of compounds consisting of various fluorinated benzoic acids was selected because of desirable nonsorbing tracer qualities. As a preliminary measurement, the melting points of five available compounds were determined to assess their general purity. The melting points, determined in a Thomas-Hoover Capillary Melting Point Apparatus (silicon oil bath), are compared with quoted values[3] in Table IV.

A high-performance liquid chromatograph, which will be used as the instrument to separate and identify the tracer compounds, was installed and is operational. We are adapting analytical methods developed at the University of Arizona for our water samples and instrument. To be useful as water tracers,

TABLE II

ANALYSES OF WELL J-13 WATER TREATED WITH G-TUNNEL TUFF

Contact Time (days)	Concentration (mg/ℓ)												
	Mg	Mn	Fe	Sr	Ba	V	Ti	Li	K	Al	Na	Si	Ca
0[a,b]	1.8	0.010	0.018	0.04	0.001	0.016	0.013	0.066	5	0.106	45	25	11
First Contact													
3[b]	0.031	0.012	0.13	0.001	0.002	0.010	0.008	0.035	2.03	0.040	58.2	26.0	0.47
7	0.044	0.017	0.21	0.002	0.003	0.010	0.008	0.056	2.59	0.057	69.1	30.0	0.68
10	0.042	0.019	0.20	0.002	0.004	0.020	0.015	0.053	2.55	0.056	70.1	29.5	0.70
21	0.031	0.021	0.19	0.002	0.004	0.022	0.012	0.058	2.72	0.046	70.5	28.8	0.59
28	0.035	0.026	0.19	0.001	0.001	0.015	0.013	0.041	2.46	0.043	70.9	29.6	0.64
Second Contact													
3	0.029	0.007	0.07	0.001	0.001	0.012	0.007	0.020	2.52	0.031	70.6	28.7	0.66
7	0.031	0.005	0.03	0.000	0.000	0.007	0.006	0.022	2.43	0.031	71.4	28.8	0.63
19	0.024	0.005	0.05	0.001	0.001	0.013	0.020	0.044	2.42	0.025	70.5	29.0	0.53
24	0.028	0.005	0.05	0.000	0.001	0.014	0.019	0.040	2.37	0.026	70.5	27.8	0.68
Mean	0.033	0.013	0.12	0.001	0.002	0.014	0.012	0.042	2.51	0.039	70.4	28.9	0.64
Std. deviation of the Sample[c]	0.007	0.009	0.08	0.001	0.002	0.005	0.005	0.014	0.11	0.013	0.7	0.9	0.06
Typical Std. Dev. of Single Analysis[d]	0.001	0.002	0.01	--	0.001	0.005	0.003	0.010	0.05	0.001	1.5	0.3	0.1
Limit of Detection	0.001	0.002	0.02	--	0.0005	0.01	0.002	0.016	0.05	0.004	3.0	0.05	0.006
Mean Concentration (mM)	1.36×10^{-3}	2.4×10^{-4}	2.2×10^{-3}	1×10^{-5}	1×10^{-5}	2.8×10^{-4}	2.6×10^{-4}	6.0×10^{-3}	6.4×10^{-2}	1.5×10^{-3}	3.06	1.03	1.59×10^{-2}

[a] Water from well J-13, not contacted with G-Tunnel rock. Composition is listed for comparison.

[b] Omitted in mean.

[c] A measure of run-to-run analytical precision, assuming that the members in the mean belong to the same sample.

[d] Within-run analytical precision based on 3 repeat measurements on a sample.

TABLE III

COMPOSITION OF WELL J-13 WATER TREATED WITH G-TUNNEL TUFF BY ANION CHROMATOGRAPHY

Contact Time (days)	Concentration (mg/ℓ)				
	F	Cl	NO_3	SO_4	HCO_3
0[a]	2.8	9.4	8.1	23	134
First Contact					
10	2.5	9.2	5.9	17.1	113
28	2.4	9.1	6.4	17.6	115
Second Contact					
3	2.3	9.6	6.4	18.1	108
7	2.3	9.7	6.0	18.2	109
Mean	2.38	9.4	6.2	17.8	111
Std. Dev. of the Sample	0.10	0.3	0.3	0.5	3
Mean Concentration (mM)	0.125	0.265	0.100	0.185	1.82

[a]Water from well J-13, not contacted with G-Tunnel rock. Composition is listed for comparison.

TABLE IV

MELTING POINTS OF WATER TRACERS

Compound (Source, Purity)	Measured Melting Point (°C)	Quoted[a] Melting Point (°C)
m-fluorobenzoic acid (Aldrich, 96%)	122.5 - 123.5	122 - 124, 124
o-fluorobenzoic acid (Aldrich, 97%)	123 - 124	123 - 125, 126.5
pentafluorobenzoic acid (Aldrich, 99%)	100.5 - 102.5	100 - 102
pentafluorobenzoic acid (Saber)	98 - 99	
α-α-α-trifluoro-m-toluic acid (Aldrich, 99%)	102 - 104	105 - 106
α-α-α-trifluoro-o-toluic acid (Aldrich, 98%)	108 - 108.5	109 - 113
3-(trifluoromethyl)-benzoic acid[b] (Saber)	104	

[a]Range is quoted by Aldrich as "typical." Single values of 124°C and 126.5°C are from Ref. 3.

[b]α-α-α-trifluoro-m-toluic acid).

the above acids, which have low solubilities in water, must be converted to soluble salts. Such a salt was prepared from 3-trifluoromethylbenzoic acid (3-TFMBA) by two methods. The first[4] involves forming the salt by adding concentrated sodium carbonate solution to the acid over a steam bath; CO_2 evolves and escapes by effervescence. The product was diluted with water, filtered, and evaporated to dryness. Later, a solution was made by dissolving a weighed portion of the salt in water. In the second method, (S. Jensen, University of Arizona, personal communication, September 1981), 0.01 M NaOH is added to a weighed amount of 3-TFMBA, and the solution stirred. The resulting solution was diluted and filtered. The two salt solutions were examined on a Hewlett Packard UV-VIS spectrometer for comparison. Although the spectra were generally similar, the fine structure between 200 and 240 nm differed. A large uv absorption band appeared in spectra of both NaOH- and Na_2CO_3-formed salts near 230 nm, corresponding to benzene-ring absorption. The pH values of the solutions were quite different. The pH of the NaOH-formed salt solution was 7.16; that of the Na_2CO_3-formed salt was 5.47. At present, the chromatographic procedure is not well enough developed to distinguish the two types of salt

C. Sorption of U(VI) (B. P. Bayhurst)

Because of the current unavailability of ^{237}U tracer, which was used in past uranium sorption experiments, a new procedure for uranium determination was developed. Natural uranyl nitrate is used as tracer; neutron activation followed by delayed-neutron counting is used for quantitative determination of uranium.

The first experiment with this technique was with G-Tunnel rock using solutions, the initial pH values of which were adjusted with hydrochloric acid or sodium hydroxide to the values listed in Table V. Results were unexpected. Sorption ratios much higher than those previously reported[5] with tuff were obtained. Values listed in Table V are from experiments with solutions traced with 1×10^{-6} M uranium and U12G-RNM9 crushed rock (<355 μm). Sorption and desorption contact times were 6 days each. Our previous sorption experiments with ^{237}U tracer generally gave R_d values <10 mℓ/g.[2,6] In addition, it should be noted that the previous experiments were performed with solutions in which dried tracer had been dissolved in the appropriate groundwater rather than with pH-adjusted solution as in this experiment.

TABLE V

U(VI) pH-ADJUSTED SORPTION RATIOS - G-TUNNEL TUFF

pH Value		R_d (mℓ/g)	
Original	Final	Sorption	Desorption
4.0	7.1	405	
4.0	6.3		2 400
6.0	7.8	137	
6.0	7.3		1 050
7.0	8.6	36	
7.0	8.6		83
8.0	8.7	18	
8.0	8.6		51
10.0	9.1	9	
10.0	8.8		43

The difference in sorption ratios with pH may be due to differences in species of uranium present. For example, Langmuir[7] has observed a variety of species at 10^{-2} atm CO_2 ranging from UO_2^{2+} in acid solution through a series of neutral and anionic complexes to $UO_2(CO_3)_4^{6-}$ in the pH range studied. Also, unusual speciation problems have been observed in our studies when americium and plutonium tracers were added in acid solution to the groundwaters and the pH of the resultant solution adjusted.[6]

A set of experiments with dried normal uranyl nitrate tracer similar to those with the ^{237}U tracer was repeated with sample JA-37. The results, given in Table VI, are in good agreement indicating that both methods of tracing with uranium for sorption experiments give the same results.

Results of experiments with G-Tunnel matrix material from hole RNM-9 using dried uranyl nitrate dissolved in groundwater are also given in Table VI. The observed sorption ratios are low but are somewhat higher than sorption ratios for U(VI) for other zeolitized tuffs[5] under ambient conditions.

TABLE VI

COMPARISON OF METHODS FOR DETERMINING U(VI)

SORPTION RATIOS (mℓ/g)[a]

Delayed-Neutron Counting[b]				^{237}U Tracer	
U12G-RNM9[c]		JA-37[d]		JA-37[d]	
Sorption	Desorption	Sorption	Desorption	Sorption	Desorption
11.4	33	5	13	4	7
11.3	35	6	13	5	7
13.0	38	6	13	5	5
11.7					
11.8					

[a]Sorption ratios for replicate measurements are reported. Uranium concentrations were 2×10^{-6} M. Contact times were 6 days.

[b]Natural uranium tracer.

[c]Particle size, ≤106 μm. Groundwaters used in preparation of traced solutions and traced solutions before contact were passed through 0.05-μm Nuclepore filters.

[d]Particle size, 335-500 μm. Solutions filtered as in footnote c, except 0.4-μm Nuclepore filters were used.

D. Crushed-Rock Column Studies (E. N. Treher and N. A. Raybold)

The crushed-rock column experiment utilizing fracture-fill material from G Tunnel was stopped after 242 days. The column was sectioned to locate the strontium, cesium, barium, and europium activities that had not been eluted (Table VII). Although most of the technetium had been eluted earlier, giving an R_d value* between 0.2 and 1.5 mℓ/g, 2.6% of the technetium loaded was still on the column, all in the last half. Approximately 20% of the ^{85}Sr, ^{137}Cs, and ^{133}Ba and >50% of the ^{152}Eu had moved away from the load point.

*The R_d of technetium could not be determined exactly because the sample volumes taken were too large to accurately obtain the volume at 50% elution.

TABLE VII

ACTIVITY REMAINING ON A COLUMN OF CRUSHED G-TUNNEL TUFF AFTER 242 DAYS

Percentage of Column in Sample	Activity Remaining (%)			
	Eu	Sr	Cs	Ba
4 (load point)	44	78	75	84
14	47	22	17	15
14	6.2		8.5	0.6
13	1.2			
16 (~ midpoint)	0.7			
12	0.6			0.5
14	0.4			
12 (exit)	0.4			

E. Fracture Flow: Block Experiments (R. S. Rundberg, S. Maestas, and A. J. Mitchell)

A sample of ash fall tuff from a 10-cm core from drill hole S80-4 in G Tunnel, containing a natural fracture, was cut into a rectangular block for future flow experiments. The block was cut with a wire saw using rock pretreated groundwater as a lubricant so that the chemistry of the rock would not be altered by the cutting operation. The sides of the block were sealed with Uralane*, a two-component polyurethane sealant. Plexiglas injection and sampling ports were sealed to the ends of the block. This block will not be submitted to stress to simulate lithostatic pressure because a previous experiment showed that tuff fractures tend to seal under stress. Water was pumped into the fracture. The polyurethane sealant proved ineffective because it did not penetrate the rock and, therefore, blistered and leaked when wet. The polyurethane seal was then coated with a 0.5-cm coating Beuhler epoxy. The epoxy coating successfully sealed the block, and the block is now being equilibrated with pretreated groundwater.

*A trademark of Furane Plastics Company.

IV. GEOCHEMISTRY OF TUFF

A. Kinetic Sorption Experiments on Wafers (E. N. Treher and N. A. Raybold)

Sorption studies of ^{85}Sr, ^{137}Cs, and ^{133}Ba on G1-1982 and G1-1883 wafers were terminated. The recent data, along with data reported last quarter,[1] are given in Tables VIII and IX. The sorption ratios for G1-1883 and G1-1982 wafers are comparable to those obtained by batch measurements on crushed, washed, and sieved (≥38 μm) samples of G1-1883 and G1-1982 tuff, reported in Sec. IV.D and in Ref. 8.

The sorption of ^{131}I on wafers of G1-1436 tuff was repeated. From preliminary measurements, it appeared that ~6% of the ^{131}I was sorbed on the wafer in 600 h. However, the counting statistics were quite poor because of the decay of the ^{131}I, so the experiment was repeated with a larger amount

TABLE VIII

SORPTION ON WAFER G1-1883

	R_d (mℓ/g)		
Time (h)	Sr	Cs	Ba
2.55	0.85	11	7.5
4.53	8.8	25	20
6.00	11	32	26
10.0	18	63	50
15.0	22	75	61
21.1	26	100	87
24.0	27	100	93
120	24	190	130
144	25	210	140
192	26	230	140
305	24	230	150
(504)[a]	(22)	(190)	(180)
869	40	230	210

[a]The numbers in parentheses are the contact time and average R_d values from batch measurements with washed fractions >38 μm (see Table XX, Sec. IV.D).

TABLE IX

SORPTION ON WAFER G1-1982

Time (h)	R_d (mℓ/g) Sr	Cs	Ba
5.0	17	65	45
7.0	30	110	78
12.0	36	180	130
16.0	45	190	170
112	84	620	580
136	86	670	560
190	88	760	560
303	84	750	650
(336)[a]	(53)	(1 120)	(670)
(504)[a]	(62)	(1 200)	(800)
860	80	1 000	710

[a]The data in parentheses are taken from Ref. 8 and are from batch measurements on crushed material that was not sieved to exclude <38 μm particles.

of ^{131}I. At 721 h no sorption was observed, and ~96% of the water in the pretreated (saturated) rock apparently had exchanged with the water that was traced with ^{131}I.

The only wafers now being studied are those of the Climax Stock and Stripa granites, G-Tunnel tuff, and G1-1436 tuff (all for sorption of ^{95m}Tc) and G-Tunnel tuff for the desorption of ^{85}Sr, ^{133}Ba, ^{137}Cs, and ^{152}Eu. No sorption of technetium has been observed on any of the wafers. With batch[9] and column measurements (Sec. IV.E) on Climax Stock granite, the sorption of technetium was quite high; however, sorption occurred only in the smallest fraction studied, 106 to 150 μm. It can be postulated that sorption of technetium may follow reduction of TcO_4^- by hematite. Perhaps in the larger fractions (and in the wafers), the hematite is encased by other mineral(s), which makes it unavailable to reduce TcO_4^-, and this coating is destroyed by crushing below 106 μm. It seems either that the iron present in the granite, which probably causes sorption of technetium by first reducing pertechnetate, is not available in the

intact rock wafers and is available after grinding or that the crushed granite was contaminated with iron during grinding because the pulverizing was done in an iron system. The latter possibility was considered in Ref. 10, where the total iron concentration in a <75-μm fraction prepared with an agate grinding system was compared with larger size fractions from an iron pulverizer. The percentage of Fe_2O_3 was 2.32 in the agate system and 2.88 to 2.33 in the other. These values were not considered to be appreciably different.[10] These results suggest that any sorption of technetium observed in crushed tuff samples may be caused by minerals not normally accessible in intact rock.

B. Actinide Sorption Studies (W. R. Daniels, F. O. Lawrence, M. R. Cisneros, P. Q. Oliver, R. D. Aguilar, and A. J. Mitchell)

Experiments comparing actinide sorption measurements using batch, circulating system, and crushed-rock column methods were described earlier,[1] and some results for americium and neptunium measurements were reported.[1] Four tuff samples were used: YM-49, a zeolitized tuff whose characterization was reported in Ref. 6; JA-37, relatively high in montmorillonite, characterization reported in Ref. 5; G1-1883, a devitrified tuff, characterization reported in Ref. 11; and U12G-RNM9, 8.1 to 10.0 ft, a zeolitized tuff, characterization reported in Ref. 11. The 106- to 250-μm fraction of crushed rock was used for all experiments.

Because neptunium sorption values tend to be small, activity in the liquid trapped in the solid portion of the sample becomes more important in calculating R_d values from data. Neptunium values have been recalculated to correct for such contribution to the activity observed in the "solid" samples (Table X).

The R_d values measured for neptunium for G-Tunnel sample U12G-RNM9 by the circulating system method are virtually the same as those determined by the batch technique. The same traced feed solution was used for both sets of measurements. The R_d values for neptunium vary with the mineralogy (Table X), ranging from 6.5 mℓ/g for sorption on the devitrified tuff to ~36 mℓ/g for sorption on the zeolitized sample from G Tunnel. As is frequently observed, the desorption R_d values tend to be higher than those for sorption.

Batch sorption measurements in air and in a controlled atmosphere (nitrogen, <0.2 ppm oxygen, <20 ppm carbon dioxide) using a neptunium-traced feed solution are in progress. Tuff U12G-RNM9 (see above), as well as tuffs YM-22 (devitrified, characterization reported in Ref. 6) and YM-38 (zeolitized,

TABLE X

COMPARISON OF NEPTUNIUM SORPTION RATIOS[a]

FROM CIRCULATING SYSTEM AND BATCH EXPERIMENTS

	R_d (mℓ/g)			
	Circulating System		Batch	
Tuff	Sorption	Desorption	Sorption	Desorption
YM-49			9(3)[b]	12(4)
JA-37			28(7)	170(50)
G1-1883			6.5(0.6)	36(10)
U12G-RNM9	34(2)	51(3)	36(5)	69(2)

[a]Nonweighted averages of sorption and desorption data from 3-, 6-, 9-, and 12-wk contact times. Rock particle size 106 to 250 μm.

[b]Values in parentheses are the standard deviations of the means.

characterization reported in Ref. 6), are being studied. The results to date are given in Table XI.

Preliminary results suggest that there may be factor of 2 differences between the controlled-atmosphere measurements and those made in air for the zeolitized tuffs YM-38 and U12G-RNM9, with sorption under reduced-oxygen conditions being greater. Duplicate samples were run where possible, and as can be seen from the standard deviations of the numbers, agreements are fairly good.

Plutonium batch and circulating system sorption and desorption contacts have been completed; however, sample counting is still in progress. Tables XII and XIII list the results for plutonium to date according to contact time and also averaged over the entire sorption period. In the batch experiments, a number of the crushed-tuff samples were pretreated with groundwater for longer periods than the routine 2 or 3 wk to investigate possible differences in sorption resulting from self-grinding of the crushed rock before start of sorption. The results are inconclusive; the majority of data for 20- and 132-day pretreatment times are in agreement. Where this is not true, the short treatment time appears to give anomalously high values, which is inconsistent with other experiments relating sorption and particle size (Sec. IV.D).

TABLE XI

COMPARISON OF RESULTS FOR NEPTUNIUM BATCH SORPTION MEASUREMENTS MADE IN AIR AND IN A CONTROLLED ATMOSPHERE

Tuff	Contact Time (days)	R_d (mℓ/g)[a] Air	Controlled Atmosphere[b]
YM-22	28.9		6.5(0.3)
	29.7	5.1	
	44.7	5.8	
YM-38	28.9		16(2)
	29.7	9.4(0.1)	
	44.7	11.0(0.2)	
U12G-RNM9	28.9		61(1)
	29.7	32(1)	
	44.7	38	

[a]Averages from duplicate analyses are given with the standard deviations of the means in parentheses.

[b]Nitrogen, <0.2 ppm oxygen, <20 ppm carbon dioxide.

TABLE XII

PLUTONIUM SORPTION DATA[a] - BATCH MEASUREMENTS

Contact Time (wk)	R_d(mℓ/g) YM-49	JA-37	G1-1883	U12G-RNM9
3	140[20][b]	300[20]	50[20]	150[100]
6	200[20]	560[20]	90[20]	290[100]
	160[132]	420[132]	50[132]	
12	820[d][20]	2 000[d][20]	110[20]	470[100]
	210[132]	760[132]	80[132]	
Average[c]	180(20)	510(100)	76(12)	300(90)

[a]All crushed-rock fraction size ranges were 106 to 250 μm.

[b]The number of days of pretreatment for a sample are given in brackets.

[c]The values in parentheses are the standard deviations of the means.

[d]Value not included in average.

TABLE XIII

PLUTONIUM SORPTION DATA[a] - CIRCULATING SYSTEM MEASUREMENTS

	R_d (mℓ/g)			
Contact Time (wk)	YM-49	JA-37	G1-1883	U12G-RNM9
4	410	260	46	450
				710
6	740	300	67	650
				1 200
12	--	320	--	1 100
Average[b]	570(170)	290(20)	56(11)	820(140)

[a]All crushed-rock fraction size ranges were 106 to 250 μm.

[b]The values in parentheses are the standard deviation of the means.

The average R_d values from batch measurements given in Table XII are consistent with those measured previously[12] with tuffs having similar mineralogies. The devitrified tuffs G1-1883, YM-54, and YM-22 gave R_d values (standard deviations) of 76(12), 84(17), and 140(40), respectively.[12] The R_d values of 180(20) and 300(90) for the zeolitized tuffs YM-49 and U12G-RNM9 are comparable to the earlier measurement of 250(90) for tuff YM-38.

Sorption results obtained from batch and circulating system measurements with plutonium are compared in Table XIV. The initial concentrations of plutonium in the feed solutions for this series of experiments were 3.1×10^{-12} M for YM-49, 4.1×10^{-12} M for JA-37, 4.1×10^{-12} M for G1-1883, and 4.8×10^{-12} M for U12G-RNM9. To eliminate any variation resulting from the preparation of the feed solutions, the same traced solution was used for both batch and circulating system contacts for a given rock. One of the initial reasons for comparing batch and circulating system results was to determine whether fine particles that were produced during pretreatment shaking of the rock in the batch procedure were leading to higher observed sorption ratios. The differences in results from the two techniques cannot readily be explained in this manner. The batch R_d value for the JA-37 tuff, which is relatively high in

TABLE XIV

COMPARISON OF PLUTONIUM SORPTION RATIOS[a]

FROM CIRCULATING SYSTEM AND BATCH EXPERIMENTS

Tuff	R_d (mℓ/g) Circulating System	Batch
YM-49	570(170)[b]	180(20)
JA-37	290(20)	510(100)
G1-1883	56(11)	76(12)
U12G-RNM9	820(140)	300(90)

[a]Nonweighted averages of sorption data from Tables XII and XIII.

[b]Values in parentheses are standard deviations of the means.

montmorillonite, appears to be higher than the value obtained with the circulating system: 510(100) vs 290(20) mℓ/g. This could be a result of the higher accessibility of the clays in the batch samples; however, the zeolitized samples YM-49 and U12G-RNM9 show somewhat lower sorption with the batch method although the accuracy of the data is poor. No large particle-size effects have been observed for sorption on zeolitized tuffs in other experiments (Sec. IV.D).

Batch studies of the dependence of plutonium sorption on concentration have been repeated using tuffs YM-22 and YM-49 (see above), as before. The results for the initial experiments were reported in Ref. 11. As nearly as possible, the feed solutions for the new experiments were prepared as were those for the earlier measurements. Variations in the "added" plutonium concentrations (Table XV) were mostly a result of differences in isotopic composition of the ^{237}Pu used and the amount of decay that occurred prior to the start of the feed preparation. Table XV lists the concentrations of the feed solutions and the resulting sorption ratios for the repeat experiment, whereas Table XVI compares the results for the two sets of samples. All available isotherm data are summarized in Table XVII. When the Freundlich equation[13] is applied to the sorption and desorption data, the parameters given in Table XVIII are obtained. As was noted in Ref. 11, within the accuracy of our results,

TABLE XV

DEPENDENCE OF PLUTONIUM SORPTION ON CONCENTRATION - NEW EXPERIMENTS

Tuff	Initial Plutonium Concentration[a] (M)		R_d (mℓ/g)[b]	
	Added	Actual	Sorption	Desorption
YM-22	7.3×10^{-12}	5.9×10^{-13}	120	2 800
	4.4×10^{-11}	2.0×10^{-11}	47	1 800
	3.7×10^{-10}	1.4×10^{-10}	79	1 400
	2.5×10^{-9}	5.7×10^{-10}	70	1 900
	2.7×10^{-8}	9.7×10^{-9}	16	910
YM-49	7.2×10^{-12}	3.1×10^{-12}	130	720
	4.4×10^{-11}	1.8×10^{-11}	240	700
	3.7×10^{-10}	1.5×10^{-10}	390	1 300
	2.5×10^{-9}	8.5×10^{-10}	2 020[c]	1 700
	3.0×10^{-8}	1.3×10^{-8}	120	560

[a]The plutonium concentrations at 100% yield, based on assay of the ^{237}Pu and ^{239}Pu solutions, are shown as "added." The plutonium concentrations actually present at the start of the batch contacts given as "actual" are lower because of losses during preparation of the feed solutions.

[b]Fraction size 75 to 500 μm.

[c]Value not included in subsequent calculations.

there appears to be little correlation between sorption ratio and element concentration in the range studied.

C. Microautoradiography Studies (E. N. Treher and N. A. Raybold)

A series of 14 filters from the preparation of feed solutions containing both ^{237}Pu and ^{239}Pu of five different concentrations were studied by microautoradiography (MAR). The solutions had been passed first through 0.4-μm Nuclepore polycarbonate filters and then through 0.05-μm filters. The differences in plutonium concentration did not affect the results obtained. All the 0.4-μm filters contained mainly colloidal or aggregated species, as well as most of the activity removed by filtering. Only one of the 0.05-μm filters contained any aggregated species, but it showed predominately single tracks. All the other

TABLE XVI

COMPARISON OF THE PLUTONIUM ISOTHERM EXPERIMENTS

		R_d (mℓ/g)[a]			
		Sorption		Desorption	
Tuff	Experiment[b]	<75 μm	75-500 μm	<75 μm	75-500 μm
YM-22	1	55(6)[c]	48(9)	950(170)	630(140)
	2		67(18)		1 800(300)
YM-49	1	180(20)	170(70)	700(60)	600(70)
	2		220(60)		990(200)

[a]Average values for all concentrations.

[b]First experiment data from Ref. 11.

[c]Values in parentheses are the standard deviations of the means.

0.05-μm filters contained single tracks only. The first 0.4-μm filter was, therefore, effective in removing essentially all aggregated plutonium species >0.05 μm.

D. Dependence of Sorption Ratio on Particle Size (S. D. Knight, E. N. Treher, and D. L. Bish)

Batch sorption ratio measurements are in progress to determine whether very small particles (<38 μm) of tuff have significantly different sorptive properties from larger particles. These experiments address the question whether small particles that are present in fractions such as the <500-μm fraction contribute significantly to the observed sorption ratios. It was anticipated that the results of these experiments would be pertinent to the interpretation of the observed differences between sorption ratios from batch and column experiments. In the latter, all material was >35 μm because of the size of the frits used.

The batch sorption experiments were done in duplicate with three different particle sizes: <38 μm, 38 to 106 μm, and 106 to 500 μm. Each fraction was washed prior to treatment on or through the appropriate sieves with water from well J-13. Six tuff samples were selected for these experiments: G1-2363, G1-2289, G1-1883, G1-3658, YM-38, and YM-54. Tracers were ^{137}Cs, ^{85}Sr, ^{133}Ba,

TABLE XVII

DEPENDENCE OF PLUTONIUM SORPTION ON CONCENTRATION - SUMMARY

Tuff	Initial Plutonium Concentration (M)	R_d (mℓ/g)[a] Sorption	Desorption
YM-22	5.9×10^{-13}	120	2 800
	8.0×10^{-12}	65	960
	2.0×10^{-11}	47	1 800
	3.0×10^{-11}	62	580
	1.4×10^{-10}	79	1 400
	2.1×10^{-10}	54	470
	5.7×10^{-10}	70	1 900
	1.8×10^{-9}	41	920
	9.7×10^{-9}	16	910
	1.0×10^{-8}	34	230
YM-49	1.6×10^{-12}	150	670
	3.1×10^{-12}	130	720
	7.7×10^{-12}	160	790
	1.8×10^{-11}	240	700
	1.3×10^{-10}	140	590
	1.5×10^{-10}	390	1 300
	4.3×10^{-10}	220	620
	8.5×10^{-10}	2 020[b]	1 700
	1.3×10^{-8}	120	560
	2.9×10^{-8}	240	340

[a]Fraction size 75 to 500 μm.

[b]Value not included in subsequent calculations.

TABLE XVIII

FREUNDLICH ISOTHERM PARAMETERS[a] FOR SORPTION AND DESORPTION OF PLUTONIUM

Tuff	Sorption			Desorption		
	n	k	Fit[b]	n	k	Fit[b]
YM-22	0.84	0.001	0.99	0.88	0.04	0.98
YM-49	0.96	0.07	0.98	1.00	0.80	0.98

[a] $y = k\ x^n$, where y_R = concentration on rock, x = concentration in solution, and n and K are constants.

[b] Coefficient of determination r^2.

and ^{152}Eu. Contacts were for 3 wk at ambient temperature under atmospheric conditions. Samples of each fraction of each rock are being analyzed by x-ray diffraction.

Available results of these experiments are given in Tables XIX and XX. For samples G1-2363 and G1-1893, both nonzeolitized tuffs, sorption ratios are higher by a factor of 2 to 4 for the smaller, <38 μm, particle size. Such a difference between particle sizes has usually been the observed difference in sorption ratios measured by batch (<500 μm) and by column experiments for nonzeolitized tuffs (Sec. IV.E).

For the zeolitized tuffs, G1-2289 and YM-38, the effect of very small particles (<38 μm) on the sorption ratios is not so noticeable as for the nonzeolitized tuffs. Sorption ratios for cesium, strontium, and barium on sample G1-2289 are very high, which is consistent with previously observed[11] relationships between sorptive behavior and mineralogy.* In any case, sorption ratios for cesium, strontium, barium, and europium are high for zeolitized tuffs, and differences in values are more difficult to observe.

Results of the x-ray diffraction analyses for some fraction sizes are given in Table XXI. For these samples, there is very little difference in mineralogic composition between the very small and the larger fractions. It seems then that the observed difference in sorption ratios for nonzeolitized

*Prior data obtained for sample G1-2289 showed rather low sorption ratios for those elements. It cannot be explained at this time why these low values were obtained.

TABLE XIX

VARIATION OF SORPTION RATIO WITH PARTICLE SIZE FOR CESIUM, STRONTIUM, BARIUM, AND EUROPIUM[a]

Tuff	Particle Size (μm)	R_d (mℓ/g) Cs	Sr	Ba	Eu
G1-2363	<38	1 390(2.3)[b]	179(2.1)	918(1.2)	5 650(4.5)
	<38	1 270(2.3)	168(2.1)	865(1.2)	5 440(4.5)
	38-106	553(2.1)	73.9(2.4)	243(1.2)	778(3.2)
	38-106	520(2.1)	62.2(2.5)	255(1.2)	794(3.2)
	106-500	414(2.1)	58.2(2.5)	230(1.2)	780(3.2)
	106-500	382(2.1)	61.4(2.5)	212(1.2)	578(3.1)
G1-2289	<38	43 400(7.3)	16 600(4.5)	173 000(6.3)	1 650(10)
	<38	27 100(5.6)	11 700(3.7)	114 000(5.2)	1 400(8.1)
	38-106	33 800(6.2)	6 340(3.1)	54 000(3.4)	780(8.8)
	38-106	29 100(5.8)	6 410(3.1)	48 500(3.3)	778(8.3)
	106-500	12 100(14)	7 830(3.2)	90 300(4.6)	817(20)
	106-500	72 100(9.3)	8 450(3.3)	69 600(4.0)	812(13)
G1-1883	<38	306(2.1)	26.2(2.8)	234(1.2)	375(3.2)
	<38	717(2.1)	80.2(2.1)	753(1.2)	653(3.4)
	38-106	198(2.1)	22.2(3.1)	208(1.2)	108(2.9)
	38-106	183(2.1)	21.7(3.1)	199(1.2)	119(3.0)
	106-500	186(2.1)	22.4(3.1)	161(1.2)	173(3.0)
	106-500	181(2.1)	21.8(3.1)	162(1.2)	153(3.1)
YM-38	<38	11 100(3.9)	13 900(3.5)	69 000(4.4)	2 250(5.6)
	<38	19 600(4.8)	20 500(4.0)	187 000(8.1)	2 990(6.9)
	38-106	16 600(4.6)	20 300(4.1)	119 000(5.9)	1 350(6.6)
	38-106	14 900(4.4)	19 600(4.0)	102 000(5.7)	1 340(6.4)
	106-500	14 300(4.3)	17 600(3.8)	56 500(4.0)	1 330(6.2)
	106-500	14 000(4.3)	17 600(3.8)	103 000(5.8)	1 510(6.2)

[a]Duplicate measurements were performed for each particle size.

[b]The values in parentheses are the standard deviations for a single measurement of R_d values expressed in per cent; these were obtained from the errors associated with the activity measurements and estimated uncertainties for the various parameters entering into the calculation. These estimated uncertainties were propagated using the rule for change of variables in a moment matrix assuming independence of the variables.

TABLE XX

AVERAGE SORPTION RATIOS FROM TABLE XXIX

Tuff	Particle Size (μm)	R_d (mℓ/g)[a] Cs	Sr	Ba	Eu
G1-2363	<38	1 330(60)	174(6)	891(27)	5 540(11
	38-106	536(17)	68(6)	249(6)	786(8)
	106-500	398(16)	60(2)	221(9)	679(101
G1-2289	<38	35 300(8 100)	14 200(2 500)	144 000(30 000)	1 530(130
	38-106	31 500(2 400)	6 380(40)	52 000(2 800)	780(1)
	106-500	42 000(30 000)	8 140(310)	80 000(10 000)	814(3)
G1-1883	<38	510(205)	53(27)	490(260)	514(140)
	38-106	190(8)	22(0)	200(5)	113(6)
	106-500	184(3)	22(0)	160(1)	163(10)
YM-38	<38	15 400(4 200)	17 200(3 300)	128 000(59 000)	2 620(370)
	38-106	15 700(900)	20 000(400)	110 000(9 000)	1 350(10)
	106-500	14 100(200)	17 300(300)	80 000(23 000)	1 420(90)

[a]Sorption ratios are given as the averages of two measurements. Numbers in parentheses are standard deviations of the means.

tuffs is due to some factor other than mineralogic composition. It was observed though that for tuff G1-2363 there was a noticeable difference in the types of feldspars in the coarse and fine fractions. Further investigations will have to be performed to determine the effects of fine particles on the sorption of radionuclides.

E. Crushed-Rock Column Studies (E. N. Treher and N. A. Raybold)

In earlier comparisons[1,6,12] of batch and column data, it has been noted that, particularly for devitrified tuffs, R_d values calculated from column data are generally several times smaller than those obtained by batch techniques. When batch measurements were repeated[8] with washed fractions of sample G1-1982, the R_d values obtained were significantly smaller (for all fractions >38 μm) than earlier measurements on unwashed fractions. Similar measurements on sample G1-1883 and G1-2363 (Sec. IV.D) also gave lower R_d

TABLE XXI

X-RAY DIFFRACTION ANALYSES OF TUFF

Sample	Particle Size(μm)	Abundance (Weight %)									
		Montmo-rillonite	Muscovite	Clino-ptilotite	Mordenite	Analcime	Quartz	Cristo-balite	Alkali Feldspar	Calcite	Glass
G1-2363	<38	5-10	<2	--	--	--	20-40	0-10	40-60[a]	--	--
G1-2363	38-106	5	<2	--	--	--	30-50	0-10	30-50[a]	--	--
G1-2363	106-500	5	<2	--	--	--	30-50	0-10	30-50[a]	--	--
G1-1883	<38	2-5	<2	--	--	--	20-40	0-10	40-60	--	--
G1-1883	38-106	<2	<5	--	--	--	30-50	0-10	30-50	--	--
G1-1883	106-500	<2	<2	--	--	--	20-40	0-10	40-60	--	--
YM-38	<38	5-15	<5	40-60	--	tr	2-10	10-20	5-15	--	--
YM-38	38-106	5-10	<5	40-60	--	--	2-10	10-20	5-15	--	--
YM-38	106-500	5-10	<2	30-50	--	tr	15-30	10-20	10-20	--	--

[a]There is a noticeable difference in the types of feldspars in the coarse and fine fractions of tuff G1-2363.

values. The batch and column results for these three tuffs are summarized in Table XXII. The results from the batch measurements of the >38-μm washed fractions are in better agreement with those from the columns than were the results of earlier comparisons. The average ratio of R_d values from batch measurements to those from column experiments for six samples is 1.1 ± 0.1. Also given in Table XXII are batch R_d values for two fractions, <38 μm and <500 μm, containing fines. These values also agree fairly well with each other, indicating that the fines present in the <500-μm sample contribute substantially to the measured sorption ratios. Sorption ratios for wafers of G1-1883 and G1-1982 tuff (Tables VIII and IX) are similar to those on the >38-μm washed fractions and significantly lower than the batch R_d values reported[11] for the <500-μm fraction.

The reason for the large effect from <38-μm particles is not known. The x-ray diffraction analyses of the various fraction sizes indicated no differences in mineralogy such as, for example, a concentration of clay in the fine fractions (Table XXI).

An experiment with a crushed-rock column, 8-cm long by 0.5-cm diam, of G1-1436 tuff, which is highly zeolitized, has been completed. Solutions of HTO and $^{131}I^-$ were passed through the column at a flow rate of ~11 m/yr to

TABLE XXII

COMPARISON OF R_d VALUES OBTAINED BY BATCH AND COLUMN TECHNIQUES FOR G1-1982 TUFF

Isotope	Tuff	Column, 38-106 μm	Batch, >38 μm, Washed	Batch, <38 μm	Batch, <500 μm	Batch[a]/Column
^{85}Sr	G1-1982	34	49-66	1 200	441	1.4
	G1-1883	30	22	53	58	0.73
	G1-2363	60	58-74	174	173	0.97
^{137}Cs	G1-1982	875	960-1 300	3 650	1 620	1.1
	G1-1883	164	181-198	510	402	1.1
^{133}Ba	G1-2363	200	212-255	413	893	1.1

[a]The ratios of batch to column R_d values were obtained by using the batch measurement in closest agreement with the columns.

investigate the effect of a very slow flow rate on the elution of I^-. There was a distinct effect. The $^{131}I^-$ had a larger apparent migration velocity than the HTO. "Anion exclusion" by materials with high cation exchange capacities whose negative charges cause an early breakthrough of the migrating anion has been reported.[14,15] The crushed-rock-column experiment should be repeated to verify the results; the elutions of HTO and I^- were identical for a number of other columns with flow rates ~2 to 3 orders of magnitude faster.[6]

A column of YM-5 tuff, with the approximate composition of 70% glass, 10% clay, 15% alkali feldspar, and 5% quartz, was prepared. After elution of ^{131}I, the column was loaded with ^{85}Sr, ^{137}Cs, and ^{133}Ba. This is the second glassy tuff run as a crushed-rock column. The first, G1-1292 tuff, a vitrophyre, gave the only broad elution curve[1] yet observed for ^{85}Sr. Another crushed-rock column prepared recently was from JA-18 tuff. Elution of ^{131}I was completed, and an experiment with ^{241}Am will be started.

Although work with crushed-granite columns is not directly related to the NNWSI, we report some of the results here because the inferences on possible sorption mechanisms may indeed have bearing on tuff. The flow through two granite columns was stopped, and the columns were sectioned and counted. One of the columns, CS-7#1, which had been loaded with ^{85}Sr, ^{137}Cs, and ^{133}Ba 2.69 yr previously, still retained 65.5% of the ^{137}Cs and 17% of the barium. The rest (34.5%) of the ^{137}Cs had been eluted in a very broad band whose peak corresponded to an R_d value of 289 mℓ/g. Of the cesium remaining on the column, 66% was still at the load point, and the rest was distributed in decreasing amounts between the load point and the exit. No cesium was detected on any of the column fittings or tubing. Cesium was not being eluted at the time the column was stopped, which implies that there is more than one mechanism for the exchange of cesium between the rock and groundwater. Of the 17% of the barium which had not been eluted and remained on the column, the majority appeared to be irreversibly sorbed; 74% was still at the load point.

The other granite-column experiment that was stopped used ^{95m}Tc and ^{152}Eu traces. After the column had been run at a flow rate of 22 m/yr for 284 days, neither ^{95m}Tc nor ^{152}Eu had been detected in the effluent. After the column was sectioned and counted, the distribution coefficients were inferred from the point at which 50% of the activities were detected. Technetium had an R_d value of 610 mℓ/g, and the R_d for europium was 759 mℓ/g. The batch R_d values

for europium were 211 to 1960 mℓ/g. The batch R_d values for technetium ranged from 32 to 160 mℓ/g on a 106- to 150-μm fraction. Larger size fractions gave 0 mℓ/g. The fraction size used in the column was 38 to 106 μm. See Sec. IV.D for a discussion of these results and for comparison with sorption ratios obtained for intact granite wafers.

F. Whole-Core Column Studies (E. N. Treher and N. A. Raybold)

Of the 22 whole-core tuff columns that we have prepared[1] for operation at low pressure with a syringe or peristaltic pump, only seven are flowing fast enough (0.1 to 0.9 mℓ/day) to be useful. Those seven are cores of G1-2410, G1-2233, G1-2854, G1-2901, G1-2698, G1-2289, and G-Tunnel tuffs. Columns G1-2698, G1-2901, G1-2854 (fracture), G1-2233, and G-Tunnel were loaded with 5-μℓ spikes of ^{85}Sr, ^{137}Cs, and ^{133}Ba and have been running for ~200 days. None of the nuclides have been detected in the effluents. This result is not surprising for the G-Tunnel, G1-2698, and G1-2233 cores, all of which contain significant amounts of zeolites (Table XXIII). Free column volumes of these cores were determined using ^{95m}Tc and ^{131}I (Ref. 8). The flow through a whole-core column of YM-54 tuff is slow, but may be used for comparison because we have done a large number and type of experiments with that particular welded tuff from the Bullfrog member of the Crater Flat Tuff. Free column volumes for cores G1-2410 and G1-2289 are now being measured with ^{131}I and HTO.

TABLE XXIII

MINERALOGY OF SAMPLES PREPARED FOR WHOLE CORE STUDIES

Sample	% Glass	% Clay[a]	% Zeolite[b]	% Alkali Feldspar	% SiO_2[c]
G1-2410	0	5-10 mnt <5 i/m	0	30-50	20-40 Qz 0-15 Cr
G1-2233	0	tr mnt 2-5 i/m	20-40 cpt 15-30 mrd	15-25	5-10 Qz 10-20 Cr
G1-2854	0	2-5 mnt 5-10 i/m	0	20-30	25-40 Qz 5-10 Cr
G1-2901	0	tr mnt 2-5 i/m	0	30-60	20-40 Qz 5-10 Cr
G1-2698	0	tr mnt 5-10 i/m	30-60 cpt	20-30	10-20 Qz 10-20 Cr

TABLE XXIII (Cont)

MINERALOGY OF SAMPLES PREPARED FOR WHOLE CORE STUDIES

Sample	% Glass	% Clay[a]	% Zeolite[b]	% Alkali Feldspar	% SiO_2[c]
G1-2289	0	tr i/m	30-50 cpt 30-50 mrd	10-20	tr Qz 2-5 Cr
G Tunnel, U12G	0	tr i/m	60-80	20-40	0
G1-3658	0	40-80 mnt	0	40-60	tr Qz 2-5 Cr
G1-1436	0	tr i/m	65-85 cpt	5-10	10-20 Qz 2-5 Cr
G1-1982	0	tr mnt	0	30-50	40-60 Cr
G1-1292	80-90	tr mnt	0	10-20	5-10 Cr
G1-3116	0	5-10 mnt 5-10 m	5-15 cpt 10-30 anal	20-30	20-40 Qz
G1-3116	0	5-10 mnt 5-10 m	5-15 cpt 10-30 anal	20-30	20-40 Qz
G1-2333	0	2-10 mnt <5 i/m	0	20-70	15-30 Qz 10-40 Cr
G1-2476	0	tr mnt 2-5 i/m	0	30-50	25-40 Qz 5-10 Cr
G1-1883	0	<10 mnt <5 m	0	50-70	30-50 Qz
YM-30	0	5-10 mnt ~5 m	30-50 cpt	30-50	40-60 Qz 5-15 Cr
YM-54	0	tr mnt tr i/m	0	~30	~60 Qz

[a] mnt = montmorillonite; i/m = illite/mica; m = mica; tr = trace.
[b] cpt = clinoptilolite; mrd = mordenite; anal = analcime.
[c] Cr = cristobalite; Qz = quartz.

G. Dependence of the Distribution Coefficient on the Freundlich Isotherm

(R. S. Rundberg)

The effects of nonlinear isotherms on sorption phenomena are being explored. Equations and computer programs to solve the diffusion equations with nonlinear

isotherms are being developed. In the course of this activity, some simple relations have been derived that can explain the dependence of the distribution coefficient (K_d) on the solution-to-solid ratio. The results of experiments[6,13] in which the solution-to-solid ratio was varied can be directly compared with the results of measurements[6,13] in which the tracer concentration was varied (isotherm determinations).

The Freundlich isotherm can be expressed by

$$\frac{x}{m} = kc^a \quad , \tag{1}$$

where

x is the number of moles of tracer in the solid,

m is the mass of the solid,

c is the final concentration of tracer in solution, and

k and a are empirical parameters.

Combining

$$K_d = \frac{x/m}{c} = kc^{a-1} \tag{2}$$

and

$$c + \frac{m}{V} kc^a = c_o \quad , \tag{3}$$

where

c_o is the initial concentration and

V is the volume of the solution ,

one obtains

$$K_d = k \left(\frac{c_o}{1 + \frac{m}{V} K_d} \right)^{a-1} \tag{4}$$

Therefore,

$$K_d^{1/1-a} \propto 1 + \frac{m}{V} K_d \quad . \tag{5}$$

For $\frac{m}{V} K_d >> 1$,

$$K_d \propto \left(\frac{m}{V}\right)^{\frac{1-a}{a}} \quad . \tag{6}$$

So the K_d dependence on the solid-to-solution ratio can be simply expressed in terms of the Freundlich isotherm parameter "a."

This simple relation seems adequate to explain the observed dependence of the R_d values on the solution-to-solid ratios. In experiments[12,13] with crushed samples of YM-22 and YM-38 tuffs, R_d values were determined using solution-to-solid ratios of 5, 10, and 30. These values were fit to the power law expression derived above, using a least-squares program. The resultant Freundlich isotherm parameters were compared with those previously determined using the standard batch technique. The comparison for sample YM-22 is given in Table XXIV. A similar comparison for sample YM-38 was not made because the

TABLE XXIV

COMPARISON OF FREUNDLICH ISOTHERM PARAMETERS DETERMINED FROM BATCH ISOTHERM AND SOLUTION/SOLID EXPERIMENTS

Sample	Size(μm)	Method	Cs	Sr	Ba	Eu
YM-22	<75	Isotherm	0.95[a]	0.76	0.82	1.45
YM-22	<75	Solution/Solid	1.01	0.83	0.83	1.1
YM-22	75-500	Isotherm	1.01[a]	0.60	0.83	1.67
YM-22	75-500	Solution/Solid	0.88	0.71	0.82	0.9

[a]These "a" values are based on measurements for a cesium concentration $<10^{-8}$ M because the initial concentrations used in the solution-to-solid experiments were $<10^{-8}$ M. Values are different from those reported originally because the cesium isotherm appears to change slope at about 10^{-6} M.

experimental uncertainties associated with high R_d values were too large to give a meaningful comparison. The agreement between the two experiments is good, with the trends being consistent and the values of "a" determined by the two methods being reasonably close.

H. Matrix Diffusion: Diffusion with Nonlinear Sorption (R. S. Rundberg)

In general, the equations that have been used to describe fracture flow with matrix diffusion and simple diffusion into tuffaceous rock treated sorption as linear with concentration.[16,17] This approach clearly has a serious deficiency because sorption on nonzeolitized tuff has already been shown to be nonlinear. The isotherm measurements[12] on tuff YM-22 show that sorption of simple cations of strontium, cesium, and barium gives a Freundlich isotherm exponent less than 1.0. A nonlinear isotherm complicates the equations for matrix diffusion by giving the diffusion coefficient a concentration dependence, rendering the differential equations nonlinear.

The formula for the apparent diffusion coefficient

$$D_{app} = \frac{D^i \varepsilon \, (\alpha/\tau^2)}{K_d \rho} \quad , \tag{7}$$

where

D^i = the ionic diffusion coefficient,
ε = the porosity,
α/τ^2 = the constrictivity-tortuosity factor,
K_d = the distribution coefficient, and
ρ = the density,

shows how the isotherm affects the diffusion coefficient. If the K_d is constant, as in the linear isotherm, the apparent diffusion coefficient remains constant. The dependence of the K_d on ion concentration for a Freundlich isotherm is shown in Sec. IV.G. The Freundlich isotherm presents special problems in the solution of the diffusion equations because, for a Freundlich isotherm parameter less than one, the K_d is infinity for a concentration of zero and the apparent diffusion coefficient is zero. In a finite-difference analysis of the problem, no diffusion can occur unless the initial concentration in the rock is greater

than zero. This means that either an arbitrary cutoff must be given to the Freundlich isotherm, below which it becomes linear, or the initial conditions must be altered to arrive at a solution. This problem does not exist for the Langmuir isotherm. The applicability of the Langmuir isotherm to our data is now being investigated.

Another phenomenon that leads to a nonlinear diffusion equation is fixation, where some fraction of the ions are irreversibly fixed in the matrix. This problem is nearly identical to that presented by Crank[18] for simultaneous diffusion with a bimolecular reaction.

A computer program, utilizing the finite difference method, is being developed to apply some of the mechanisms to matrix diffusion. Eventually, the program will be incorporated into a transport model so that a more realistic model can be developed.

I. Matrix Diffusion and Related Solute Transport Properties of Fractured Tuff

(G. R. Walter, R. D. Golding, and G. M. Thompson)

1. Tuff Porosities. Pore-size distribution measurements have been completed on 10 tuff samples using mercury infusion porosimetry. The porosimetry procedures and data reduction techniques are described in Ref. 1. The pore-size measurements were made for pores with theoretical diameters (based on the Washburn equation) ranging from 10^{-1} to 10^{-5} cm.

To summarize the porosimetry data, the volume of mercury intruded at each pressure was divided by the total volume intruded at the maximum porosimeter pressure (approximately 2000 psi). The fractional volume intruded for each sample was then multiplied by 100 to obtain the cumulative percentage of porosity for pores with diameters $>10^{-5}$ cm. The Washburn equation was then used to compute the theoretical pore diameter corresponding to each measured pressure. These data were used to construct the pore-size distribution curves shown in Fig. 1.

As can be seen from Fig. 1, nearly all of the porosity in these samples is due to pores $<10^{-2}$ cm in diameter. In most of the samples, over 50% of the porosity is due to pores $<10^{-4}$ cm (1 μm) in diameter. Possibly half of the samples contain a large fraction of their porosity in pores $<10^{-5}$ cm in diameter.

Measurements of grain density are in progress for the tuff samples for which the pore size distributions were determined. Until the grain density measurements have been completed, we cannot compute the total porosity of these

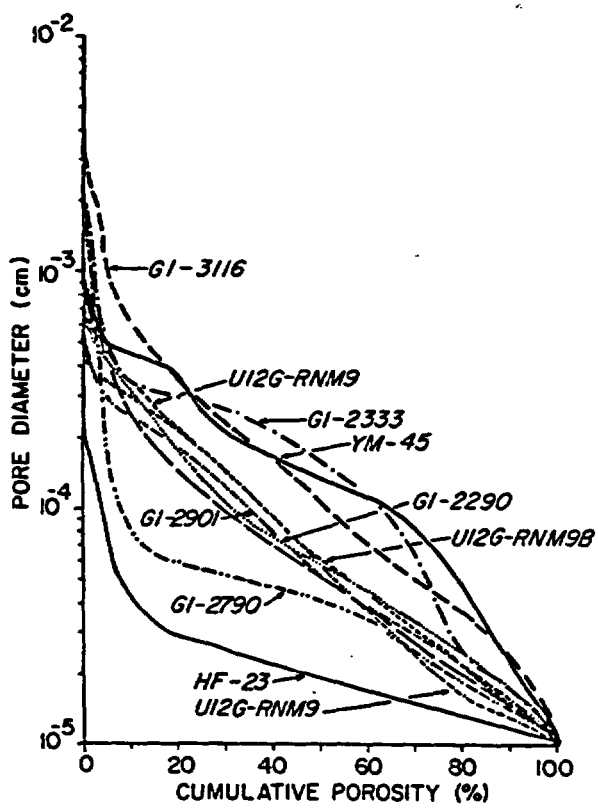

Fig. 1. Cumulative pore-size distributions for NTS tuff samples.

samples and construct total pore-size distribution curves. A preliminary evaluation of the extent to which the pore volumes determined from the porosimetry approach the total pore volumes of the samples can be made, however, by comparing the apparent grain densities computed from the porosimeter measurements to grain densities for other tuffs from the Nevada Test Site (NTS) determined by Manger.[19] To make this comparison, we have listed in Table XXV the measured bulk densities, apparent porosities (total intrusion volume/bulk volume), and apparent grain densities for our samples. Manger reported that grain powder densities for samples of the Paintbrush tuff ranged from 2.2 to 2.5 g/cm^3 with an average of ~2.33 g/cm^3. If one assumes that the grain powder density of the grains composing the tuffs at the NTS is relatively uniform, then the apparent grain densities in Table XXV give an indication of the portion of the pore volume that we could not measure on our porosimeter. Specifically, Table XXV shows that samples G1-2233, G1-2290, HF-23, U12G-RNM9 (5.9 to 6.4 ft), and U12G-RNM9 (16.2 ft to 17.5 ft) all have apparent grain densities <2.2 g/cm^3, implying that substantial fractions

TABLE XXV

BULK DENSITIES, APPARENT POROSITIES, AND APPARENT GRAIN DENSITIES FOR NTS SAMPLES

Sample (Date)	Bulk Density (g/cm^3)	Apparent Porosity	Apparent Grain Density (g/cm^3)
G1-2233 (9/16/81)	1.45	0.272	1.99
G1-2901 (9/17/81)	2.01	0.152	2.38
KT-23 (9/18/81)	1.46	0.100	1.62
U12G RNM9B (9/23/81) (5.9 ft to 6.4 ft)	1.48	0.147	1.73
U12G RNM9 (9/25/81) (16.2 ft to 17.5 ft)	1.31	0.225	1.69
G1-2290 (7/1/81)	1.64	0.246	2.17
G1-2290 (9/28/81)	1.57	0.191	1.94
G1-2790 (10/1/81)	2.04	0.153	2.40
YM-45 (10/2/81)	1.99	0.176	2.41
G1-2333 (10/2/81)	1.68	0.285	2.36
G1-3116 (10/5/81)	1.81	0.227	2.34

of the pore volumes were not measured. The other samples have apparent grain densities ranging from 2.34 to 2.41 g/cm^3, implying that most of the porosity of these samples was measured.

2. Diffusion Studies. Measurements have been made of the effective diffusion coefficient of NaBr through tuff samples U12G-RNM9 (5.9 to 6.4 ft, Side B, Position A) and YM-45. The measurements were made using the steady-state technique and apparatus described in Ref. 1. The measured values are shown in Table XXVI, and the diffusion curves from which these values were calculated are shown in Figs. 2 and 3. Much of the variation of the observed diffusion curve from the regression line in these figures appears to be due to diurnal temperature variation in our laboratory, which affects the output from the ion selective electrode. This problem will be corrected by continuously monitoring the solution temperature near the electrodes using our data acquisition computer and applying a temperature correction to millivolt readings. The ratio of the effective diffusion coefficient to the free aqueous diffusion coefficient for NaBr is also listed in Table XXVI. The difference in the

TABLE XXVI

EFFECTIVE DIFFUSION COEFFICIENTS FOR NaBr

Sample	Initial Concentration (M)	D_e (cm^2/s)	D_e/D_o [a]
U12G-RNM9 (5.9 ft. to 6.4 ft.)	4.95×10^{-2}	$1.15 \times 10^{-6} \pm 1.8 \times 10^{-8}$	0.07
YM-45	4.89×10^{-2}	$1.93 \times 10^{-6} \pm 4.1 \times 10^{-8}$	0.12

[a] D_o is the free aqueous diffusion coefficient of NaBr.

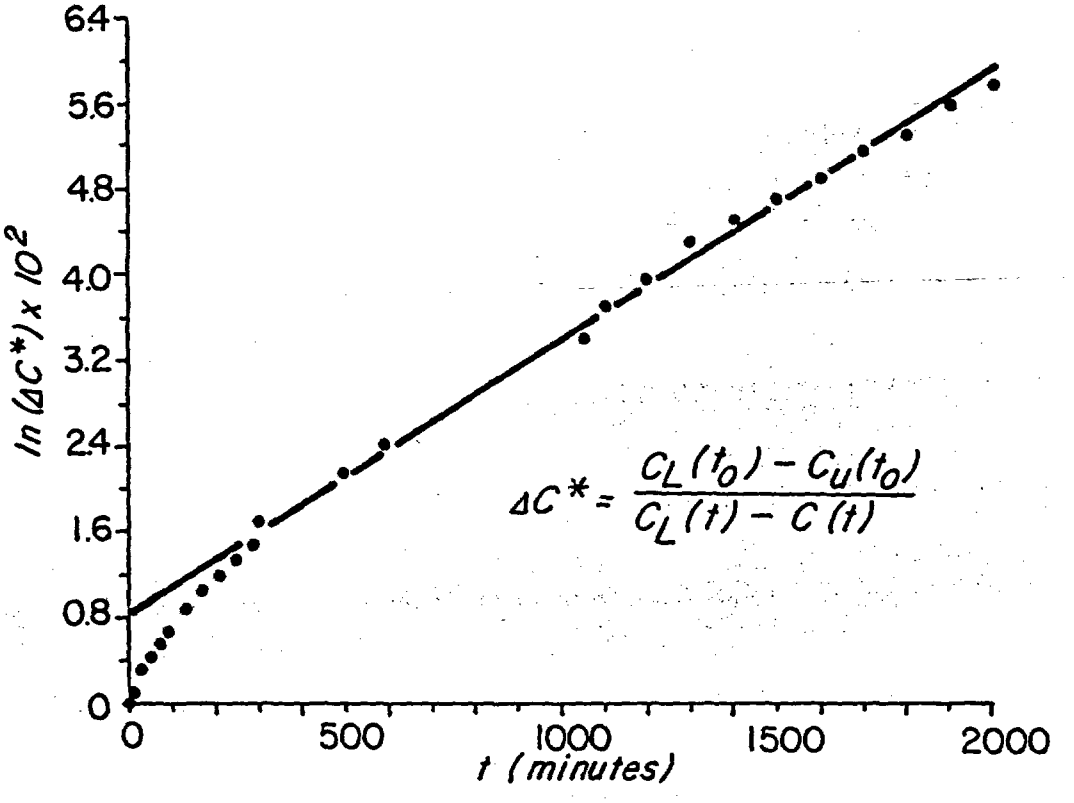

Fig. 2. Time-concentration curve from diffusion test on sample U12G-RNM9 (5.9 to 6.4 ft, Side B).

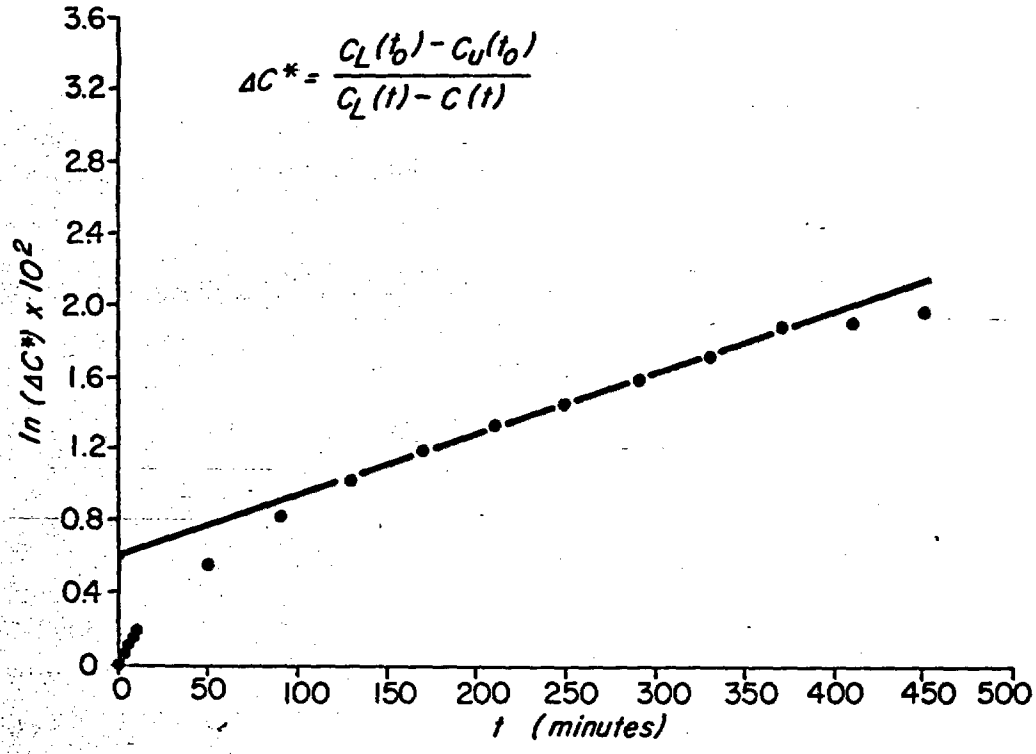

Fig. 3. Time-concentration curve from diffusion test on sample YM-45.

effective diffusion coefficients between these two samples may in part be explained by the differences in their median pore diameters. From Fig. 1 we see that the median pore diameter of U12G-RNM9B is ~0.62 μm, whereas that of YM-45 is ~1.7 μm. Their measured porosities, however, are nearly the same.

Because the mercury porosimetry measurements on sample YM-45 indicated that the measured porosity of 0.18 is close to the true porosity, we can make a further calculation from the diffusion data, using the relationship between the effective diffusion coefficient and the free aqueous diffusion coefficient given by Porter and others.[20]

$$D_e = \alpha\theta(L_e/L)^2 D_o \quad , \tag{8}$$

where

D_e = the effective diffusion coefficient,

α = an empirical coefficient related to electrical surface interactions,

θ = the porosity, and

L_e/L = the tortuosity.

If we assume that $\alpha \cong 1$ because of the high ionic strength of the solution, then calculate the tortuosity to be 1.2, as compared to a maximum value for a porous medium composed of spherical particles of 1.4.

3. Tracer Characterization: Acid Dissociation Constants. The dissociation constants of the five fluorinated benzoic acid tracers were determined by potentiometric titrations using an Altex PHI 71 pH meter and double-junction glass membrane electrode. Accurate pK_a values for these tracers are necessary to predict their diffusion properties.

All titrations were performed using a 9.700×10^{-3} M NaOH solution prepared from water distilled over $KMnO_4$ and degassed with nitrogen. Potassium chloride was added to the solution to adjust the ionic strength to ~0.1 M. The alkali solution was stored under a nitrogen atmosphere in a 5-ℓ polyethylene bottle wrapped with aluminum foil. Solutions of primary standard potassium acid phthalate and the fluorinated benzoic acids were prepared in a similar manner with their ionic strengths adjusted to 0.1 M with KCl. The concentrations of the acids ranged from 4×10^{-3} M for the weakest and least soluble acid to 10^{-2} M for the strongest.

The titrations were performed under a nitrogen atmosphere using the apparatus shown in Fig. 4. The pH electrode was standardized with Curtis Matheson pH 4 and pH 7 buffer solutions. The base solution was standardized against the potassium acid phthalate solutions.

The dissociation constants for the acids were then determined from the titration curves using the following mass balance and mass action equations.

$$K_a = \frac{a_{H^+}\, a_{A^-}}{a_{HA}} \quad , \tag{9}$$

$$m_{HA} = F_{HA} - m_{H^+} + m_{OH^-} - F_{B^-} \quad , \tag{10}$$

$$m_{A^-} = F_{B^-} + m_{H^+} - M_{OH^-} \quad , \tag{11}$$

$$a = \gamma m \quad , \tag{12}$$

where

- a = the activity,
- m = the molarity,
- F = the formal concentration,
- γ = the activity coefficient,
- HA = the undissociated acid,
- H^+ = the hydrogen ion,
- A^- = the acid anion,
- B^- = the base, and
- OH^- = the hydroxide ion.

Equations (9) through (12) are combined to give

$$K_a = \frac{a_{H^+}\ \gamma_{A^-}\ (F_B + a_{H^+}/\gamma_{H^+})}{\gamma_{HA}(F_{HA} - a_{H^+}/\gamma_{H^+} - F_{B^-})} \quad . \tag{13}$$

The activity coefficients γ_{H^+}, γ_{A^-}, and γ_{HA} used in the calculations were 0.83, 0.77, and 1.0, respectively.[21] The dissociation constants were determined by solving Eq. (13) for four to five points in the buffer region of the titration curve. The computed pK_a values are given in Table XXVII with their standard

TABLE XXVII

MEASURED AND REPORTED pK_a VALUES FOR FLUOROBENZOIC ACIDS

Acid	pK_a Value	
	Reported (25°C)	Measured (23°C)
Benzoic	4.19[a]	4.18 ± .01
p-fluorobenzoic	4.04[b]	4.13 ± .01
m-fluorobenzoic	3.85[b]	3.82 ± .01
o-fluorobenzoic	2.90[b]	3.42 ± .02
m-trifluoromethylbenzoic	--	3.79 ± .01
pentafluorobenzoic	1.73[c]	1.49 ± .02

[a] Ref. 22.
[b] Ref. 23.
[c] Ref. 24.

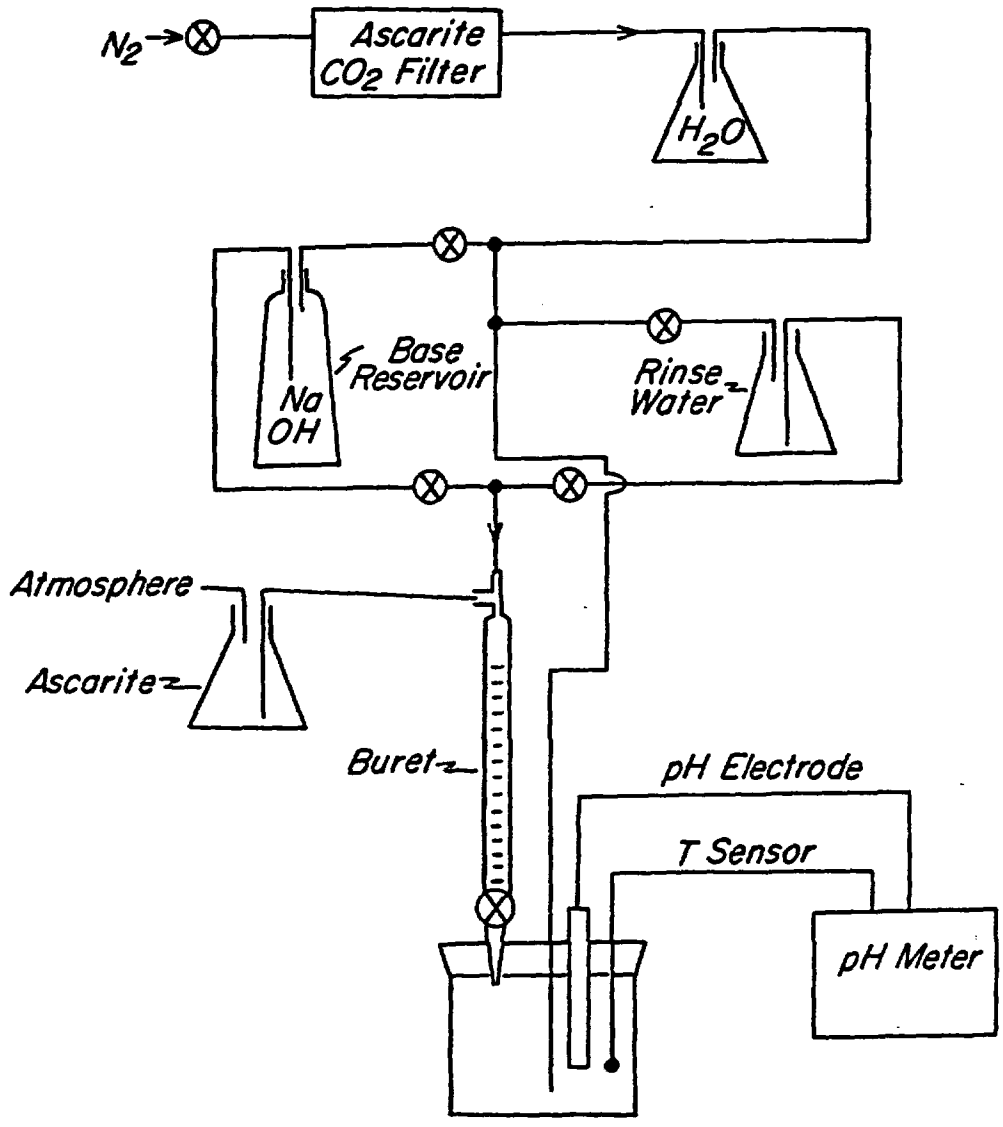

Fig. 4. Apparatus for performing pH titrations under nitrogen atmosphere.

errors and the reported values.[22-24] The relative strengths of the acids can be qualitatively predicted from the expected stability of the respective anions or the ability of each to accommodate the negative charge. The charge of the benzoate ion is distributed over most of the molecule through resonant stabilization. All the possible resonant structures can be represented by the hybrid shown in Fig. 5.

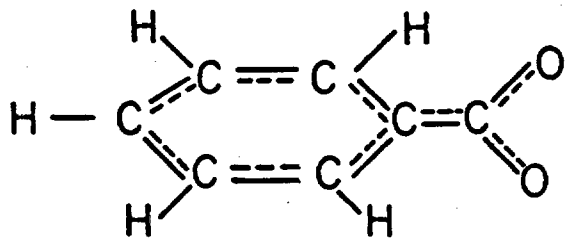

Fig. 5. Resonance hybrid structures for benzoate anions.

When an electron-withdrawing fluorine is added to the ring, the ability of the ring to accept the charge from the carboxyl group is enhanced. The effect of electron-withdrawing substituents diminishes with distance, and this tendency is observed with the o, m, and p isomers. The three fluorines attached to the m-methyl group in m-trifluoromethylbenzoic acid produce an electron-deficient carbon, which in turn withdraws electrons from the ring about the same as the single fluorine. As expected, the fully substituted pentafluorobenzoic acid is the strongest acid by 2 orders of magnitude. The pK_a of pentafluorobenzoic acid is lower than previously reported, possibly because of poor standardization of the electrode below pH 4. The reproducibility of values at different points in the titration was less than for the weaker acids. The only explanation of the disagreement between reported and measured values for the o-fluorobenzoic acid is impurities in the acid. This could be checked by titrating a solution made from a recrystallized sample.

J. Fracture Flow: Laboratory Experiments with Isolated Fractures

(R. S. Rundberg, J. L. Thompson, S. Maestas, and A. J. Mitchell)

We monitored the elution of ^{85}Sr and ^{137}Cs through two fractured tuff samples taken from cores from the USW-G1 drill hole at the NTS. The tuff samples, G1-2335 and G1-2840, are welded tuffs from the Bullfrog and Tram members, respectively. The cores are 2.54-cm diam by 4.76-cm long and contain tensile fractures (artifical fractures). Forty-milliliter "slugs" of groundwater traced with ^{85}Sr and ^{137}Cs were passed through the fractures.

The breakthrough curves were compared with the theoretical curves predicted by the analytic solution to flow through a one-dimensional fracture coupled to diffusion into the matrix.[16] The fracture volume and the fracture aperture, in particular, were determined using Darcy's law.[25] The tuff samples were not placed under confining pressure because the samples were found to seal under moderate pressure (~1000 psi), whereupon the fracture permeability was reduced to the same magnitude as the matrix permeability.

The flow through the fracture was straight flow, enabling direct comparison with the one-dimensional calculations. The parameters used in the one-dimensional calculations are given in Table XXVIII.

In Figs. 6 through 13, experimental values are compared with theoretical curves. The theoretical curves were obtained by substituting R_d values from batch measurements (called "batch K_d values" in this section) for the K_d values in the calculations and using a lower value to get a closer fit to the experimental results.

The results of the fracture-flow experiments with tuff samples from cores G1-2335 and G1-2840 were not in agreement with the calculation obtained when the batch K_d values were used (Figs. 6, 8, 10, and 12). The K_d values that gave the best fits (Figs. 7 and 9) to the breakthrough portion of the strontium elution were 30 mℓ/g and 16 mℓ/g for samples G1-2335 and G1-2840, respectively. The batch measurements yielded 148 mℓ/g and 160 mℓ/g for samples G1-2335 and G1-2840, respectively. A general trend observed in sorption experiments of

TABLE XXVIII

PARAMETER VALUES USED TO CALCULATE ELUTION CURVES

Parameter[a]	G1-2335	G1-2840
ρ_s	1.71	2.02
α/τ^2	0.1	0.1
U_f	2.85×10^{-2} cm/s	2.76×10^{-2} cm/s
2b	30.7 μm	31.7 μm
x	4.76 cm	4.75 cm
ε	0.312	0.191

[a]Terms defined in Sec. III.F, Ref. 8.

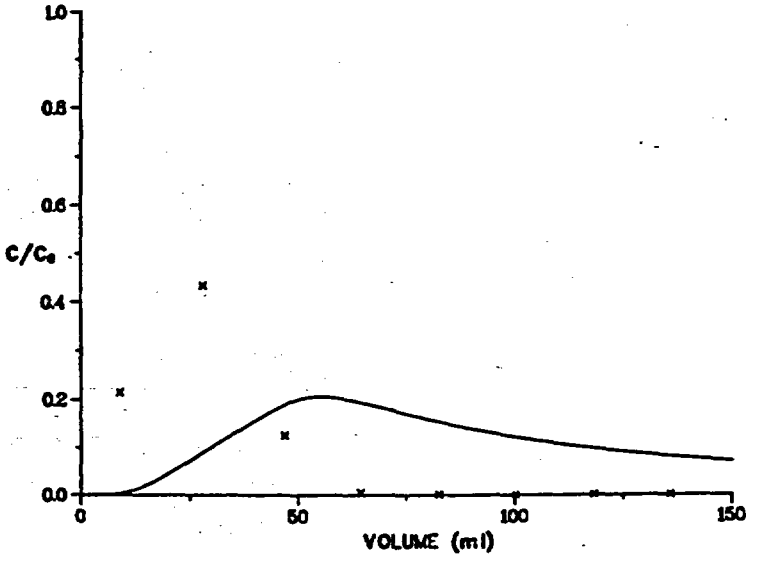

Fig. 6. Elution of a 40-mℓ slug of ^{85}Sr in groundwater through a tuff (G1-2335) fracture. Theoretical curve (solid line) assumes the experimental batch K_d (148 mℓ/g). The points (x) represent experimental data.

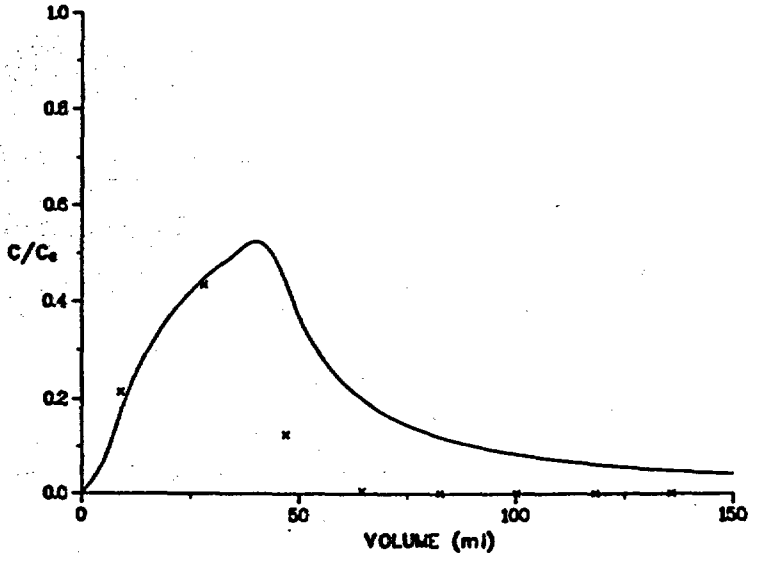

Fig. 7. Elution of a 40-mℓ slug of ^{85}Sr in groundwater through a tuff (G1-2335) fracture. Theoretical curve (solid line) assumes K_d = 30 mℓ/g. The points (x) represent experimental data.

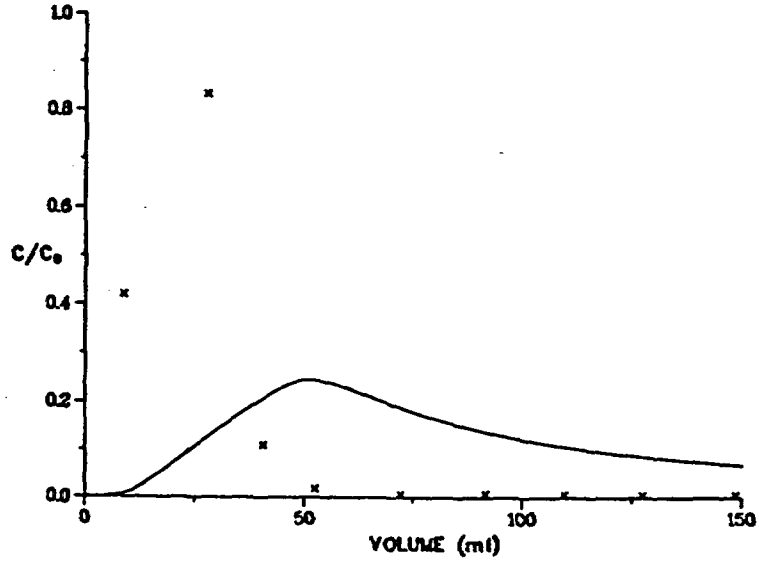

Fig. 8. Elution of a 40-mℓ slug of ^{85}Sr in groundwater through a tuff (G1-2840) fracture. Theoretical curve (solid line) assumes the experimental batch K_d (165 mℓ/g). The points (x) represent experimental data.

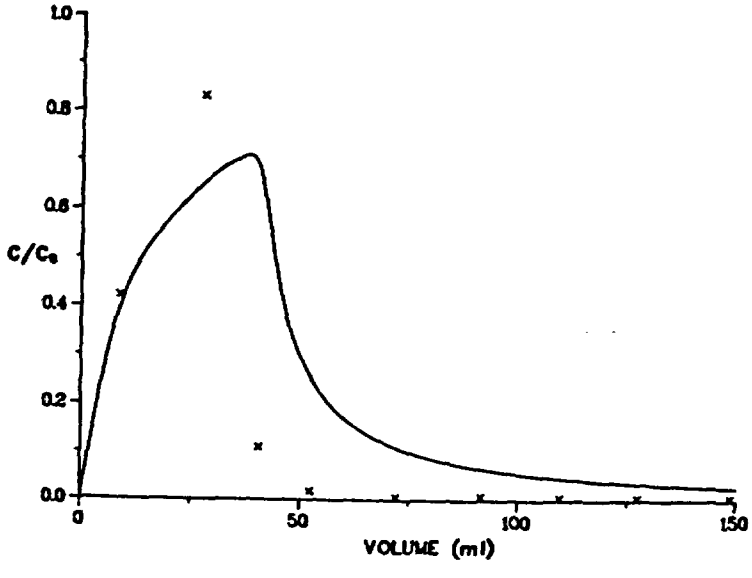

Fig. 9. Elution of a 40-mℓ slug of ^{85}Sr in groundwater through a tuff (G1-2840) fracture. Theoretical curve (solid line) assumes K_d = 16 mℓ/g. The points (x) represent experimental data.

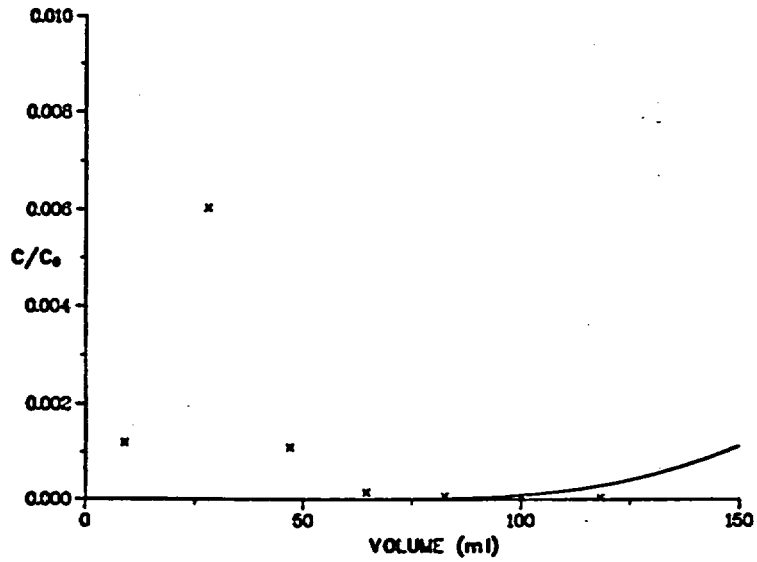

Fig. 10. Elution of a 40-mℓ slug of ^{137}Cs in groundwater through a tuff (G1-2335) fracture. Theoretical curve (solid line) assumes the experimental batch K_d (1100 mℓ/g). The points (x) represent experimental data.

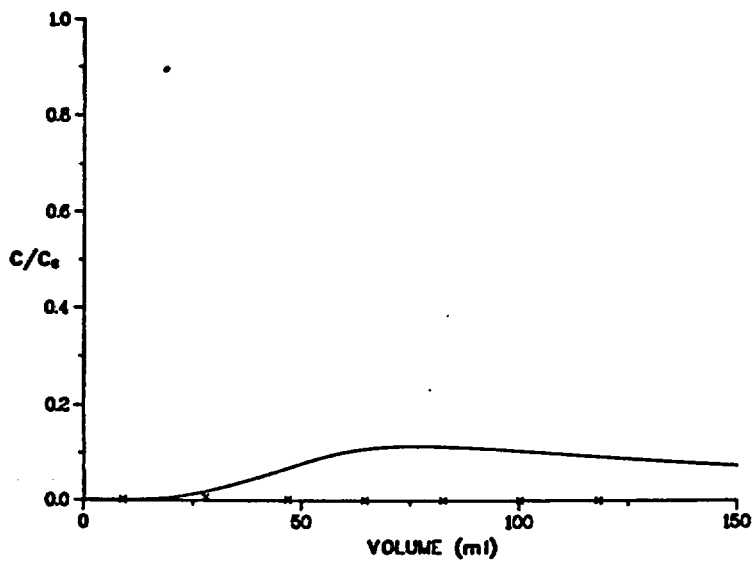

Fig. 11. Elution of a 40-mℓ slug of ^{137}Cs in groundwater through a tuff (G1-2335) fracture. Theoretical curve (solid line) assumes K_d = 220 mℓ/g. The points (x) represent experimental data.

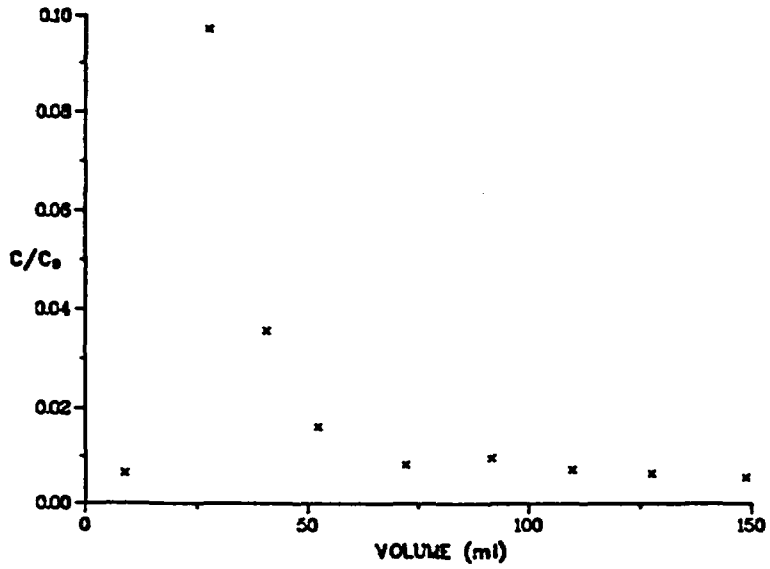

Fig. 12. Elution of a 40-mℓ slug of ^{137}Cs in groundwater through a tuff (G1-2840) fracture. The theoretical curve, which is too low to be visible on the same scale as the experimental data, assumes the experimental batch K_d (2200 mℓ/g). The points (x) represent experimental data.

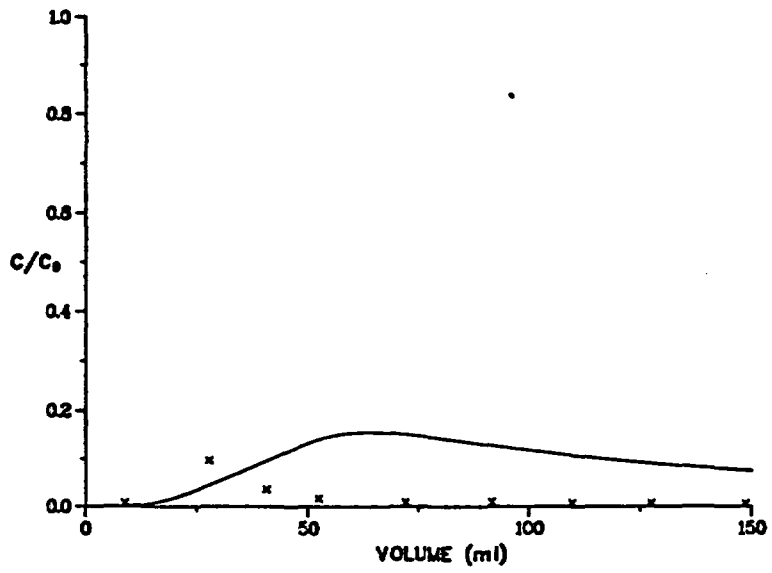

Fig. 13. Elution of a 40-mℓ slug of ^{137}Cs in groundwater through a tuff (G1-2840) fracture. Theoretical curve (solid line) assumes K_d = 110 mℓ/g. The points (x) represent experimental data.

tuff is that batch measurements yield K_d values that are 3 to 5 times larger than the K_d values that are determined by column experiments. These experiments were consistent with that trend. In addition, the shape of the elution calculated for the tuffs is not in agreement with the observed elution. The activity desorbs more slowly than would be expected for reversible, diffusion-controlled sorption. This observation is also consistent with previous measurements of sorption on tuff. In general, the K_d values determined by desorbing activity from tuff are considerably larger than those determined from the sorption process. The values from the cesium runs do not fit even when K_d values are lowered. When the batch K_d values were used, the expected peak arrival time was off-scale with respect to the experimental peak (Figs. 10 and 12). Lowering the K_d values, however, brought the peak arrival time closer to the experimental, but the area under the curve became greater than the experimental curve (Figs. 11 and 13). In conclusion, a satisfactory fit to the experimental elution curves for cesium could not be achieved using the simple matrix diffusion model.

K. Behavior of Pu(IV) Polymer (J. L. Thompson and V. L. Rundberg)

The migration of radiocolloids through geologic media is of interest because a number of fission-product and transuranic species can exist in polymeric forms or as pseudocolloids. We initiated a study of Pu(IV) polymer with the ultimate goal of investigating its interaction with tuff and its potential for migrating through porous and fractured tuff. The immediate goal of this study was to characterize the behavior of dilute Pu(IV) polymer solutions using the techniques of centrifugation, filtration, and microautoradiography.

A stock solution of Pu(IV) polymer, ~5×10^{-3} M in Pu(IV) and ~4×10^{-2} M in $HClO_4$, which was provided by T. W. Newton, had been purified on a cation exchange column, and its characteristic absorption spectrum had been verified. For most of the work reported below, this stock solution was diluted with 4×10^{-2} M $HClO_4$ to a Pu(IV) concentration in the 10^{-6} M range. Centrifugations were done at 12 000 rpm (28 000 g) for 1 h. Filtrations utilized 13-mm-diam Nuclepore polycarbonate filters with pore sizes 0.4 μm and 0.05 μm. Kodak NTB-3 nuclear track emulsion was employed in the microautoradiography and was applied either to glass slides on which the Pu(IV) solution had been dried or to filters that had contacted the plutonium aqueous phase. The presence of

aggregated species in aqueous phases or on filters was indicated by "stars" and dense spots on the autoradiographs. These aggregates may include polymeric species, colloids, and pseudocolloids.

The following observations were made concerning Pu(IV) polymer in 0.04 M $HClO_4$.

1) Neither the 0.4-μm nor the 0.05-μm polycarbonate filters appeared to be effective in removing the polymer from the aqueous phase. Plutonium was sorbed on these filters to some extent, as indicated by numerous single tracks in the autoradiographs, but the general absence of stars showed that effective removal did not take place.
2) Centrifugation at 28 000 g removed a large fraction of the polymeric material. Treatment of the centrifuged material in an ultrasonic bath caused it to be redispersed to approximately its original concentration.
3) The conditions under which solutions are dried may affect the appearance of autoradiographs. In general, a solution containing polymers dried on glass gives rise to more and larger stars than does that solution dried on a polycarbonate filter.

The observation with respect to the inefficiency of the filters is in agreement with work by Lloyd and Haire,[26] who reported that 95% of plutonium colloids formed in a nitrate solution passed through 0.01-μm Millipore filters. Other workers,[27] however, have reported the successful use of filters with Pu(IV) colloids. Neither of these groups examined the filters with microautoradiography.

The observed efficiency of high speed centrifugation for removing substantial amounts of polymeric Pu(IV) agrees with literature reports.[28] An "order-of-magnitude" calculation based on our centrifuge geometry and the assumption of a colloid particle density of ~6 g/cm^3 indicates that particles of diameter $\gtrsim 5 \times 10^{-3}$ μm were removed during centrifugation.

The use of microautoradiography to identify the presence of polymers can be extremely useful. However, as this study illustrates, one must be aware that the stars found in the autoradiographs may be artifacts caused by aggregates produced in the solution drying process. We are continuing our efforts to develop techniques for quantifying dilute radiocolloids.

L. Plutonium Chemistry in Near-Neutral Solutions: The Pu(IV) Polymer

(T. W. Newton and V. L. Rundberg)

The existence of bright green suspensions of Pu(IV) polymer has been known for a long time.[29] The Pu(IV) polymer is of interest for environmental reasons and because it is probably related to the nonreactive Pu(IV) that we have observed to form in very dilute solutions.[1]

We have prepared suspensions of the polymer by diluting Pu(IV) in HCl-$HClO_4$ mixtures, rather than by using nitric acid as previously described.[26,27] We observed the formation of polymer to be much slower than reported for nitric acid solutions,[30] but after ionic species were removed with a cation exchange resin, the spectra of our preparations were essentially the same as those reported.[30] In a second method of preparing the polymer, we partially neutralized Pu(IV) in $HClO_4$ with NaOH solution, followed by heating to 90°C for 30 min. The spectrum of the suspension prepared in this way and treated with a cation exchange resin agreed with published spectra.

The solubility of the polymer is very important for environmental considerations. It may be defined in terms of the equilibrium

$$\underset{\text{polymer}}{(1/n)(PuO_2 \cdot mH_2O)_n} + 4H^+ = Pu^{4+} + (2 + m)H_2O \qquad (14)$$

In a previous attempt to measure the solubility,[27] polymer was equilibrated in solutions with $3 \leq pH \leq 7$. Soluble plutonium was defined as all plutonium species that pass through a Centriflo filter with 2-nm pore size. These species were shown to be predominantly Pu(V) although the oxidizing agent was not identified.

We have performed a preliminary experiment to test the feasibility of determining the solubility of the Pu(IV) polymer in a way that should avoid the difficulties associated with the method described above. We mixed PuO_2^{2+} with polymer at pH 3, where the equilibrium reaction is probably

$$(1/n)(PuO_2 \cdot mH_2O)_n + PuO_2^{2+} = 2PuO_2^{+} + (m)H_2O \qquad (15)$$

The concentration of PuO_2^{2+} was determined spectrophotometrically as a function of time. The question to be answered is whether or not concentrations can be identified where the rates of the forward and reverse reactions are equal. If

so, the equilibrium quotient for reaction (15) can be determined and that of reaction (16) calculated from it by using the Pu^{4+} - PuO_2^+ and the PuO_2^+ - PuO_2^{2+} potentials.

Three mixtures were prepared in 10^{-3} M $HClO_4$: (A) 10^{-4} N polymer, (B) 5 x 10^{-5} M PuO_2^{2+}, and (C) 10^{-4} N polymer and 5 x 10^{-5} M PuO_2^{2+}. The mixtures were put into 10-cm absorption cells, and the concentrations of PuO_2^{2+} were determined spectrophotometrically at 830 nm for 30 days.

Mixture (A) showed an increase in PuO_2^{2+} concentration corresponding to <0.01% per day based on the total plutonium present. In an experiment in much higher acid, a mixture ~5 x 10^{-3} N in polymer and 0.04 M in $HClO_4$ was followed spectrophotometrically for 18 days. During this period, the Pu(VI) concentration increased at a rate of ~0.11% of the total plutonium per day.

Mixture (B) showed a linear decrease in PuO_2^{2+} concentration because of the net reaction

$$2PuO_2^{2+} + H_2O = 2PuO_2^+ + 2H^+ + \tfrac{1}{2}O_2 \qquad (16)$$

caused by alpha particle self-irradiation from the decay of the ^{239}Pu. The observed rate of this reaction was 1.25% of the total plutonium per day. This is in satisfactory agreement with the value of 1.5% per day reported for solutions in 1 M $HClO_4$.[31]

The mixture of PuO_2^{2+} and polymer, mixture (C), showed a nonlinear decrease in PuO_2^{2+} concentration. The absorbance values were found to agree within 0.002 with the empirical equation

$$A = 0.325 \exp(-0.0299\ t) - 0.050 \quad , \qquad (17)$$

where A is the absorbance and t is the time in days. The initial decrease in absorbance, from this equation, is 0.0097 per day or 3.5% of the original Pu(VI) per day, or 1.16% per day based on the total plutonium present.

At the end of 30 days, excess Ce(IV) was added to estimate the ionic plutonium species present. The $Ce(ClO_4)_4$ added was such that the final mixtures were 3 x 10^{-4} M in Ce(IV) and 0.079 M in $HClO_4$.

Mixture (A), polymer with no added PuO_2^{2+}, showed a rapid absorbance increase of 0.03 during the first minute after the Ce(IV) was added. This was followed by a much slower increase with a rate of about 2.5 x 10^{-4} per day for

the next 150 min. These results indicate that Ce(IV) reacts relatively slowly with the polymer, but ~5% of the plutonium present reacted rapidly. This suggests that small amounts of ionic Pu(III), Pu(IV), or Pu(V) had formed.

Mixture (B), PuO_2^{2+} with no polymer, reacted rapidly with Ce(IV). The final absorbance value was reached within 1 min and remained constant for the next 163 h. The PuO_2^{+} formed in reaction (3) was apparently reoxidized to PuO_2^{2+}

Mixture (C), polymer plus PuO_2^{2+}, showed a rapid increase in absorbance when the Ce(IV) was added, followed by a slower increase similar to that observed for mixture (A). The absorbance, extrapolated to the time the Ce(IV) was added, was greater than that of the original mixture. The concentrations of PuO_2^{2+} in mixture (C) before and after adding the Ce(IV) were calculated from the absorbance values and are given in Table XXIX, along with two derived quantities.

Entry d in Table XXIX shows that reaction (15) occurred at a slow but measurable rate. From entry e, it can be calculated that the average rate of reaction (16) was 0.67% per day based on the total plutonium present. This is about one-half the rate observed for mixture (B), where no polymer was present. This smaller value indicates that some of the alpha particles from the the decay of the ^{239}Pu are absorbed in the colloidal particles and do not lead to chemical reaction.

Because the results in Table XXIX show that most of the reduction of PuO_2^{2+} was by reaction (16), an accurate estimation of the equilibrium quotient for reaction (15) cannot be expected. In addition, an assumption about the rate of reaction (16) must be made. The calculation will be made, however, to show what is involved. Equation (17) can be used to show that the observed rate of reduction of PuO_2^{2+} equaled the average rate of reaction (16) at about 18.5 days. If the rate of reaction (16) was essentially constant in the mixture containing the polymer as well as in mixture (B), then the net rate of reaction (15) must have been zero at about 18.5 days. At this time, the rates of the forward and reverse reactions would have been equal, and the equilibrium quotient, $Q = [PuO_2^{+}]^2/[PuO_2^{2+}]$, can be calculated from the concentrations for that time. The value obtained in this way is about 4×10^{-5} M, with an experimental uncertainty of 20%.

TABLE XXIX

PuO_2^{2+} CONCENTRATIONS IN A MIXTURE OF Pu(IV) POLYMER AND PuO_2^{2+}

Description	Concentration ($M \times 10^5$)
a. Original mixture	4.86
b. After 30 days, room temperature	1.40
c. After adding Ce(IV); extrapolated to time of mixing	5.34
d. Consumed by reaction (15), (c)-(a)	0.48
e. Consumed by reaction (16), (a)-(b)-(d)	2.98

The potentials for the Pu^{4+} - PuO_2^+ and the PuO_2^+ - PuO_2^{2+} have been estimated to be 1.115 V and 0.933 V, respectively, at an ionic strength of zero.[32] These lead to $[Pu^{4+}][PuO_2^{2+}]/[PuO_2^+]^2[H^+]^4 = 1.2 \times 10^3\ M^{-4}$. Combining this with our provisional estimate of 4×10^{-5} M for $[PuO_2^+]^2/[PuO_2^{2+}]$ gives $5 \times 10^{-2}\ M^{-3}$ for reaction (14).

The result obtained above is reasonable, so it may be concluded that the experiment should be repeated using ^{242}Pu to minimize the complexities caused by reaction (16).

M. Storage Capacity and Permeability (C. J. Duffy)

The method of measuring permeability has been modified so that the storage capacity as well as the permeability of a specimen can be determined. Storage capacity is the additional volume of fluid that can be stored in a unit volume of rock by a unit increase in pore fluid pressure. The storage capacity is a function of both the porosity and the compressibility of the pores. When the fluid pressure in the pores is increased, the amount of fluid stored is increased by compression of the fluid and enlargement of the pores.

Analysis of the measurements of various tuff samples is still being refined; however, the values of both permeability and storage capacity are surprisingly low when compared to granitic rocks. The values for tuff and granite are nearly equal although those for tuff tend to be slightly higher. This result is surprising because granitic rock porosities are typically 1% or less, and tuff porosities are generally in the 10 to 40% range. Further, in a given rock,

permeability varies roughly as the cube of the porosity. Clearly the pore structures of granites and tuffs differ considerably.

The similarity in storage capacity is also surprising. Almost all the storage capacity of a granite is a result of the compressibility of the pores; it has very little pore volume in which to store fluid by compression. Approximately half the storage capacity of a typical tuff arises from fluid compression. The pore compressibility is roughly equal for the two rock types. Although increasing the effective confining pressure on a granite from 0 to 30 MPa may decrease the porosity a factor of 2, the effect of such a change on a tuff would be negligible.

Examination of tuff in thin section generally shows large round pores. This is clearly the nature of most of the porosity of tuff. However, if channels the size of the pores existed through the tuff, the permeability of the tuff would be much higher than is observed. There must be, rather than continuous large channels, large pores connected by a network of small channels that constrict the fluid flow. Further, to account for the low pore compressibility, the large pores in particular, and perhaps even the small channels, must be rather round in cross section.

Refinement of a model for the pore structure of tuff will not only enhance understanding of its permeability but will aid in understanding diffusion into the bulk rock. Very preliminary evidence indicates that the observed permeability may be a function of the distance over which permeation occurs. Relating this observation to the pore structure may indicate whether or not such a dependence can be expected in diffusion coefficients.

H. Anion Analyses of Groundwaters (P. L. Wanek and K. Wolfsberg)

Refinement of parameters for ion chromatography continued. The detector response above ~30 mg/ℓ carbonate is not linear. Nonlinearity is especially troublesome in comparing samples from a controlled atmosphere with air-exposed samples. Because the carbonate solution peak is broad, greater sensitivity in distinguishing concentration differences can be obtained by running dilute samples at a comparatively high instrumental sensitivity setting.

An HP-3390A integrator was connected to the ion chromatograph for digitizing the detector output for anions of strong acids. In general, instrumental conditions have now been determined that will permit both detection of usually low-level components, such as nitrate and phosphate, to concentrations as low

as 1 mg/ℓ, and also detection of higher level, higher response components, such as chloride and sulfate. Because the chloride peak is strong in comparis to the peaks of other anions, samples with chloride concentrations $\gtrsim$20 mg/ℓ have to be rerun for chloride alone at a lower sensitivity setting or be diluted. If not, a signal overrun is flagged on the integrator. So, in some cases, dilutions and multiple injections of samples must be made for optimum sensitivity of both types of components.

O. Groundwater Analysis (A. E. Ogard, S. Maestas, A. J. Mitchell, and P. L. Wanek)

Water samples have been taken at two different times separated by 35 days of pumping from well UE25b-1 at Yucca Mountain. These samples were returned to Los Alamos for chemical analysis. The results of the cation and anion analyses are listed in Table XXX.

At the time of sampling on August 7, 1981, water from the well was also introduced into a closed stirred cell where the Eh, pH, $E_{S^{2-}}$, temperature, and oxygen content were measured (Table XXXI).

The -75 mV output of the sulfide electrode indicates the concentration of S^{2-} or HS^- is $<<10^{-10}$ M and probably is due to the sulfide in the electrode's membrane. The relationship between Eh and $E_{S^{2-}}$, however, may be a useful measure of oxygen poisoning[1] and should be ~180 mV if the electrodes are not poisoned and oxygen is absent. Our Eh-$E_{S^{2-}}$ value of 295 mV is too large, so perhaps the Eh electrode was poisoned by air. On the other hand, it is reasonable to have a positive Eh value indicating an oxidizing water because the water from the well was still foaming, indicating that all the drilling fluids, which originally contained air, had not been eliminated from the water in the well. Similar measurements were not made during the later sampling because the well water was still foaming.

It has been shown[11] that unfiltered waters or even waters filtered through 0.45-μm membranes contain suspended iron solids that can be removed on further filtration through 0.05-μm Nuclepore membranes. As expected, the filtering step through 0.05-μm Nuclepore membranes reduced the iron content drastically for both of the water samples collected 35 days apart. No other large differences between samples was noted due to this filtration step.

The acidification step after filtration appeared to result in a slight increase in the concentration of virtually all the cations. Whether or not this is reproducible is not known at this time. The increased cation content,

TABLE XXX

CATION AND ANION ANALYSES OF WELL UE25b-1 WATER

	Concentration (mg/ℓ)					
	Sampled August 7, 1981			Sampled September 11, 1981		
Element[a]	Not Filtered	Filtered[b]	Filtered,[b] Acidified	Not Filtered	Filtered[b]	Filtered,[b] Acidified
Mg	0.740	0.719	0.833	0.606	0.586	0.677
Mn	0.192	0.185	0.193	0.004	0.005	0.004
Si	30.1	29.3	31.6	28.1	28.8	31.5
Fe	0.154	0.029	0.047	0.34	0.025	0.035
Sr	0.051	0.050	0.055	0.041	0.042	0.046
Ba	0.005	0.004	0.005	0.006	0.006	0.007
V	0.010	0.010	0.011	0.006	0.013	0.015
Ti	0.023	0.018	0.015	0.014	0.022	0.026
Ca	20.4	20.2	22.5	17.3	17.6	19.7
Li	0.834	0.818	0.873	0.262	0.257	0.283
K	3.62	3.45	3.69	3.19	3.13	5.28
Al	0.044	0.016	0.032	0.015	0.015	0.028
Na	59.8	58.1	63.02	53.6	53.2	55.8
F		1.1			1.2	
Cl		11.4			7.2	
NO_2		N.D.[c]			N.D.	
PO_4		N.D.			N.D.	
NO_3		N.D.			0.6	
SO_4		21.1			20.6	
CO_3		118			118	

[a]The notation does not imply the species in solution.

[b]0.05-μm Nuclepore membrane.

[c]N.D. = not detected.

TABLE XXXI

RESULTS OF FIELD ANALYSES OF WELL UE25b-1 WATER

Measurement	Value
Eh	220 mV referenced to a H_2 electrode
pH	7.2
$E_{S^{2-}}$	-75 mV referenced to a H_2 electrode
Temperature	36.8°C
O_2	oxygen electrode did not function

however, is not from the acid itself because J. T. Baker Ultrex HNO_3 was used. Metallic impurities in this acid are all <30 ppb, and only 2 mℓ of acid was used in 50 mℓ of solution.

Two large changes can be noted in cation concentration with length or time of pumping. The lithium content decreased greatly, as expected. Lithium chloride had been added during the well drilling to serve as a tracer to show when the well had been pumped enough to infer that formation water was being pumped from the well. However, the lithium content after more than 13 million gallons had been pumped was still not down to background levels of ~0.050 mg/ℓ. The manganese content also decreased drastically between the two pumpings. No reason for this can be offered at this time.

P. Modeling of Groundwater Interactions (J. F. Kerrisk)

The results of a preliminary search for free-energy data at 25°C for some of the mineral phases found during exploratory drilling at or near Yucca Mountain are described in the Appendix. The reactions of primary interest are the formation of the minerals from aqueous species. Equilibrium-constant or free-energy data are presented for these formation reactions from a particular basis set of aqueous species. Data were found for silica (crystalline and amorphous forms), alkali feldspars, some clays, and one zeolite (analcime). No data were found for three other zeolites observed at Yucca Mountain: clinoptilolite, heulandite, and mordenite. Free-energy data were estimated for these minerals by three different techniques. Many of the minerals of interest actually exist as solid solutions; however, few thermodynamic data are available for solid solutions.

The data presented in the Appendix are all for simple compounds with specific compositions.

V. MINERALOGY-PETROLOGY OF TUFF

Studies of Drill Cores from USW-G2 and UE25b-1H (D. L. Bish, F. A. Caporuscio, B. M. Crowe, B. Arney, D. Broxton, G. H. Heiken, R. E. Semarge, R. C. Gooley, and D. T. Vaniman)

Drill hole USW-G2 was recently completed by NNWSI personnel to a depth of 6000 ft, at a spot north of the exploration block in Yucca Mountain; also, drill hole UE25b-1H was completed to a depth of 4000 ft, just north of the previous shallower drill hole UE25a-1. Samples from both of these new drill holes recently became available, and our detailed mineralogic and petrologic studies of these samples will be completed during the second quarter of FY-1982. Therefore, a much more thorough discussion of these cores will be presented in the next quarterly report. However, the x-ray diffraction studies of cores from both of the new drill holes are complete and the results can now be presented.

Results of the x-ray diffraction studies of USW-G-2 and UE25b-1H are significantly different from the previous study of USW-G1. Some of the outstanding differences involve the distribution of zeolite minerals, critical to the naturally sorptive barriers proposed in most tuff-based repository models. Unlike USW-G1, and unlike the previously studied drill holes at Yucca Mountain, USW-G2 contains a prominent zeolitized horizon well above the present water table. This horizon is marked by 10 to 90% clinoptilolite-rich tuff at depths of 548 to 762 ft in USW-G2. These depths include most of the Pah Canyon Member and the uppermost Topopah Spring Member of the Paintbrush Tuff. It is possible that the densely welded zone high in the Topopah Spring Member may have acted as a local aquitard, creating a perched water table that would cause extensive zeolitization this high in the section. The suggestion of a perched aquitard is reinforced by the absence of abundant zeolites from 770 to 1536 ft, below the aquitard zone described and including almost the entirety of the central Topopah Spring Member, which is somewhat less welded and should be readily zeolitized if saturated.

Clinoptilolite again occurs in abundance at 1634 ft in USW-G2 and remains abundant to a depth of 2430 ft. This depth interval includes the lowermost Topopah Spring Member and most of the bedded tuff of Calico Hills. This is

also a zone of abundant mordenite mineralization (1691 to 2667 ft). Below this interval is a gap of approximately 300 ft, unzeolitized, and corresponding to welded zones within the Prow Pass Member of the Crater Flat Tuff. Dense zeolitization again occurs in the lowermost 200 ft of the Prow Pass Member (3067 to 3250 ft). The last abundant occurrence of clinoptilolite in USW-G2 is at 3250-ft depth, and the last abundant occurrence of mordenite is at 3578 ft. These final occurrences are at the base of the Prow Pass Member and at the base of the Bullfrog Member (Crater Flat Tuff), respectively.

The deepest occurrences of the sorptive zeolites clinoptilolite and mordenite are shallow in USW-G2, compared with USW-G1. In drill hole USW-G1, clinoptilolite last occurs at 3850 ft, below the Tram Member of the Crater Flat Tuff. In USW-G1 the last abundant occurrence of mordenite is at 2622 ft. Thus there are at least two major differences between the zeolite distributions in USW-G2 and USW-G1: zeolites are abundant in restricted zones above the water table in USW-G2, and the depth distributions of zeolites are much shallower in USW-G2 than in USW-G1.

Details of zeolite, other mineral, and glass distributions are presented in Table XXXII for USW-G2 and in Table XXXIII for UE25b-1H. Table XXXIII only contains data for the depth interval below 2400 ft in UE25b-1H; the interval above 2400 ft in this locale is covered in a previous report.[33] In UE25b-1H the last occurrence of clinoptilolite in abundance is at 3092 ft (upper Tram Member), and the last occurrence of mordenite in abundance is at 2919 ft (also within the upper Tram Member). Thus the deepest occurrences of abundant highly sorptive zeolites are shallowest in UE25b-1H, almost as shallow in USW-G2, and deepest in USW-G1.

The less sorptive zeolite analcime can occur through the breakdown of more hydrous zeolites (for example, clinoptilolite) under the effect of increased temperature.[34] Such alterations could lead to the facies-like overlapping assemblages of clinoptilolite-mordenite tuff and analcime tuff in USW-G1 and USW-G2. In UE25b-1H, however, there is a 200-ft gap between the last appearance of the more hydrous zeolites (clinoptilolite at 3092 ft) and the first appearance of analcime (3298 ft). This gap may be significant in evaluating conflicting hypotheses concerning the origins of zeolites at Yucca Mountain: either the zeolites may form in a system relatively closed to solution exchange but under a high thermal gradient, or the zeolites may form in an open system of downward-percolating cation-charged waters under a lower thermal gradient. This question will be dealt with in the forthcoming report on USW-G2.

TABLE XXXII

X-RAY DIFFRACTION ANALYSES OF TUFF FROM DRILL HOLE USW-G2 (WEIGHT PERCENT)

Sample[a]	Depth (m)	Smectite	Mica	Clinoptilolite	Mordenite	Analcime	Quartz	Cristobalite	Alkali Feldspar	Calcite	Other
USW-											
G2-10	3.0		5-10					30-50	30-50		10-20[b]
G2-100	30.5		<5					30-50	30-50		10-25[b]
G2-200	61.0							30-50	30-50		5-15[b]
G2-230	70.1							30-50	30-50		5-15[b]
G2-270	82.3	2-10						30-50	30-50	15-30	
G2-304	92.7						5-10	30-50	30-50		10-20[b]
G2-331	100.9	30-50							30-50	10-20	
G2-338	103.0	40-60							5-10		30-50[c]
G2-358	109.1	15-30					Tr.	5-10	20-40		20-40[c]
G2-395	120.4	5-15	<2				<5	10-20	15-30		30-50[c]
G2-501	152.7	5-20	<3					5-10	10-20		40-60[c]
G2-547	166.7	5-15	<5					5-15	10-20		40-60[c]
G2-548	167.0		<5	5-10				20-40	30-50		
G2-561	171.0	10-20	<3	10-20				20-40	25-40		
G2-627	191.1	5-15	<5	10-20				20-40	30-50		
G2-675	205.7	30-50	<5	15-30				5-10	15-30		
G2-723	220.4	5-15	<5					<5	5-10	30-50	15-30[c]
G2-743	226.5	30-50	<5	<5			5-15	5-15	10-20	5-15	15-30[c]
G2-762	232.3	2-5		75-90				5-15	<5		10-20[b]
G2-770	234.7	<2	5-10					15-30	60-80		
G2-822	250.5	5-10	<5					20-40	30-50		10-20[b]
G2-855	260.6	<5	2-5					20-40	30-50		5-15[b]
G2-898	273.7	<2	2-5	<5				20-40	40-60		5-10[b]
G2-921	280.7	10-20					20-40	15-30	20-40	5-10	
G2-951	289.9	<2					15-30	20-40	20-40		
G2-984	299.9	2-10					15-30	10-20	15-30	15-30	
G2-1032	314.6	2-10	<2				15-30	20-40	20-40		
G2-1072	326.7	2-10	<2				20-40	5-15	30-50		
G2-1133	345.3	5-15	<2				15-30	20-40	40-60		
G2-1178	359.1	<5	<2				10-25	20-40	30-50		

TABLE XXXII (Cont.)

X-RAY DIFFRACTION ANALYSES OF TUFF FROM DRILL HOLE USW-G2 (WEIGHT PERCENT)

Sample	Depth (m)	Smectite	Mica	Clinoptilolite	Mordenite	Analcime	Quartz	Cristobalite	Alkali Feldspar	Calcite	Other
G2-1234	376.1	2-10					10-25	20-40	30-50		
G2-1281	390.4	5-15					15-30	15-30	30-50		
G2-1331	405.7	5-15					15-30	20-40	30-50		
G2-1382	421.2	5-15	<2				15-30	15-30	40-60		
G2-1420	432.8	5-15					15-30	20-40	30-50		
G2-1461	445.3	5-15					10-20	30-50	30-50		
G2-1536	468.2	10-20		<5			10-20	30-50	30-50		
G2-1585	483.1	5-15		<5			10-25	20-40	30-50		
G2-1634	498.0	30-50	<2	30-50				15-30			
G2-1664	507.2	<2		<2			5-10	5-10	10-20		50-70[c]
G2-1691	515.4	5-15		40-60	5-10			15-25	5-15		
G2-1745	531.9	10-20		30-50	5-10		5-10	15-30	10-20		
G2-1752	534.0	5-15		50-70	5-10		<5	5-15	5-10		
G2-1798	548.0	<2		40-60	15-30		5-15	10-20	15-30		
G2-1848	563.3			40-60	15-30		Tr.	15-30	10-20		
G2-1899	578.8	<2	<2	40-60	15-30		5-10	10-20	10-20		
G2-1952	595.0		<5	5-10	40-60		10-20	10-20	10-20		
G2-2001	609.9		<2	5-10	40-60		10-20	10-20	15-30		
G2-2078	633.4	<5	<5	20-40	20-40		5-10	10-20	10-20		
G2-2158	657.8	<5	<5	20-40	15-30	Tr.	5-10	15-30	10-20		
G2-2248	685.2	<5	<2	20-40	20-40		5-15	15-30	15-30		
G2-2353	717.2	<2	2-10	5-15	20-40		15-30	15-30	10-20		
G2-2430	740.7	<5	5-15	20-40	5-15		20-40	0-10	20-40		
G2-2528	770.5	<5	5-15	<5	15-30		20-40	<5	20-40		
G2-2667	812.9	<5	5-10		20-40		15-30	<5	30-50		
G2-2744	836.4	<5	<2				30-50	5-10	40-60		
G2-2820	859.5	<2	<2				20-40	2-10	50-70		
G2-2869	874.5	<2	2-5				20-40	2-5	50-70		
G2-2887	880.0	<5	<2				20-40	2-5	50-70		
G2-2950	899.2	2-10	<3				20-40	2-10	40-60		
G2-2970	905.3	5-15	<3				30-50	0-10	40-60		

TABLE XXXII (Cont.)

X-RAY DIFFRACTION ANALYSES OF TUFF FROM DRILL HOLE USW-G2 (WEIGHT PERCENT)

Sample	Depth (m)	Smec-tite	Mica	Clino-ptilolite	Morden-ite	Anal-cime	Quartz	Cristo-balite	Alkali Feldspar	Calcite	Other
G2-3037	925.7	30-50	<2		<5		20-40	0-5	15-30		
G2-3067	934.8		<2	5-10	20-40			20-40	20-40		
G2-3192	972.9	5-10		20-40	5-15	Tr.	20-40	0-5	20-40		
G2-3250	990.6	15-30	<2	5-15	5-15	20-40	15-30	0-5	15-30		
G2-3308	1008.3	2-5	10-20				15-30	0-10	40-60		
G2-3330	1015.0		2-10				20-40	0-10	50-70		
G2-3330(F)	1015.0	5-15	2-10				10-20		15-30		40-60[d]
G2-3349	1020.8	<2	2-10				15-30	0-10	50-70		
G2-3366	1026.0	<2	2-10				20-40	0-10	50-70		
G2-3416	1041.2	<2	2-10				20-40		50-70		
G2-3454	1052.8	20-35	<5		15-30	Tr.	15-35		15-35		
G2-3492	1064.4	10-25	<5		15-30	5-10	20-40		15-30		
G2-3512	1070.5	10-20	5-10		2-10	10-20	20-40		30-50		<5[e]
G2-3541	1079.3	5-15	5-10			20-40	20-40		15-30		<5[e]
G2-3578	1090.6	15-30	5-15		15-30		20-40		15-30		
G2-3627	1105.5	10-20	5-15			<5	20-40		30-50		
G2-3671	1118.9	5-15	5-10			5-10	20-40		30-50	5-10	<2[e]
G2-3720	1133.9	5-15	5-10			Tr.	20-40		30-50		
G2-3724	1135.1	20-30	<5				30-50		20-40		<5[b]
G2-3750	1143.0	20-30	5-15				20-40		30-50		
G2-3772	1149.7	15-30	5-10				20-40		30-50		
G2-3795	1156.7	25-40				<2	30-50		20-40		<5[e]
G2-3833	1168.3	20-40	2-10				20-40		20-40		
G2-3875	1181.1	20-30	5-10			<5	30-50		15-30		
G2-3908	1191.2	10-25					20-40		30-50	2-10	
G2-3933	1198.8	10-20				20-40	20-40		20-40	5-10	
G2-3968	1209.4	10-25	2-10			Tr.	30-50		30-50		Tr.[e]
G2-4005	1220.7	10-20	5-15			<5	15-30		30-50	5-10	

TABLE XXXII (Cont.)

X-RAY DIFFRACTION ANALYSES OF TUFF FROM DRILL HOLE USW-G2 (WEIGHT PERCENT)

Sample	Depth (m)	Smectite	Mica	Clinoptilolite	Mordenite	Analcime	Quartz	Cristobalite	Alkali Feldspar	Calcite	Other
G2-4090	1246.6	15-30	10-25			2-10	15-30		20-40	5-15	
G2-4167	1270.1	10-20	10-20			<2	15-30		30-50	5-15	<5[e]
G2-4199	1279.9	10-20	5-15			Tr.	10-25		30-50	10-25	<2[e]
G2-4209	1282.9	5-15	5-10			2-10	10-25		40-60	<5	
G2-4267	1300.6	10-20	5-10			<5	20-40		30-50	<5	
G2-4329	1319.5	5-15	2-10			<5	20-40		30-50	5-15	
Pumice											
G2-4467	1361.5	15-30					15-30		30-50	5-15	
G2-4467	1361.5	5-15	2-10			<5	15-30		30-50	5-15	
G2-4570	1392.9	5-15	5-10			<5	20-40		30-50	10-25	
G2-4788	1459.4	10-20	<5			Tr.	20-40		30-50	5-15	
G2-4805	1464.6	10-30				Tr.	30-50		30-50		
G2-4816	1467.9	15-30				Tr.	30-50		20-40	2-10	
G2-4838	1474.6	15-30				<5	20-40		30-50	2-10	
G2-4873	1485.3	20-40				<2	20-40		20-40		
G2-4885	1488.9	20-40					20-40		20-40	<5	
G2-4893	1491.4	15-30	5-10			<2	20-40		20-40		
G2-4924	1500.8	10-25	5-15			<5	20-40		20-40	5-10	
G2-4949	1508.5	30-50	5-15				15-30		15-30		
G2-5017	1529.2	10-30					20-40		30-50		<5[e]
G2-5017(S)	1529.2	2-10					30-50		30-50	2-10	<5[e]
G2-5029	1532.8	10-30	10-30				20-40		20-40		
G2-5144	1567.9	2-10	10-30				20-40		30-50	2-10	
G2-5171	1576.1	10-25	20-40				15-30		15-30	2-10	
G2-5206	1586.8	10-20	10-25			Tr.	15-30		30-50		2-10[e]
G2-5213	1588.9	5-15	5-15				20-40		20-40	2-10	5-15[e]
G2-5305	1617.0	5-15	5-15				15-30		30-50	5-15	<2[e]
G2-5369	1636.5	5-15	10-20				20-40		30-50	5-15	
G2-5379	1639.5	2-10	10-20				20-40		30-50	5-15	
G2-5434	1656.3	2-10	15-30			<2	15-30		30-50		
G2-5493	1674.3	<5	15-30				20-40		30-50	10-20	

TABLE XXXII (Cont.)

X-RAY DIFFRACTION ANALYSES OF TUFF FROM DRILL HOLE USW-G2 (WEIGHT PERCENT)

Sample	Depth (m)	Smec-tite	Mica	Clino-ptilolite	Morden-ite	Anal-cime	Quartz	Cristo-balite	Alkali Feldspar	Calcite	Other
G2-5505	1677.9	5-15	10-20				15-30		30-50	5-10	2-10[f]
G2-5538	1688.0	15-35					15-30		20-40	10-25	5-15[f]
G2-5596	1705.7	10-20					15-30		30-50	2-10	5-10[f]
G2-5638	1718.5	10-25				Tr.	10-25		30-50	10-25	2-10[f]
G2-5657	1724.3	20-40					15-30		20-40	2-10	2-10[f]
G2-5696	1736.1	10-20				<2	15-30		30-50	10-25	5-15[f]
G2-5762	1756.3	5-15					15-30		30-50	15-30	5-15[f]
G2-5820	1773.9						15-30		30-50	2-10	10-25[f]
G2-5885	1793.7	10-25					15-30		10-25	20-40	2-10[f]
G2-5895	1796.8	10-25					20-40		20-40	15-30	2-10[f]
G2-5918	1803.8	5-15					30-50		30-50		2-10[d], 2-5[f]
G2-5926	1806.2	10-20				Tr.	30-50		30-50		
G2-5931	1807.8	15-30					15-30		30-50	2-10	5-15[e]
G2-5951	1813.9	15-30				<2	20-40		30-50	2-10	<5[e]
G2-5971	1820.0	10-25				<5	20-40		30-50		
G2-5992	1826.4	10-25				<5	30-50		30-50	2-10	<5[e]

[a] F = Fracture; S = Spherulite
[b] Tridymite
[c] Glass
[d] Hematite
[e] Kaolinite
[f] Chlorite

TABLE XXXIII

X-RAY DIFFRACTION ANALYSES OF TUFF FROM DRILL HOLE UE25b-1H (WEIGHT PERCENT)

Sample[a]	Depth (m)	Smec-tite	Mica	Clino-ptilolite	Morden-ite	Anal-cime	Quartz	Alkali Feldspar	Calcite	Kaolinite	Other
UE25b-											
1H 2402	732.1	10-20	2-10				30-50	30-50			
1H 2450	746.8	5-15	5-10				30-50	30-50	2-10		
1H 2525	769.6	5-15	5-15				30-50	30-50			
1H 2596	791.3	5-15	2-10				30-50	30-50	2-10		
1H 2651	808.0	5-15	2-10				30-50	30-50			
1H 2737	834.2	2-5	2-10				20-40	40-60			
1H 2832	863.2	10-20	2-10	2-5	10-25		15-30	20-40	2-5		
1H 2855	870.2	10-25	2-5	2-5	10-25		15-30	20-40	2-10		
1H 2867	873.9	10-25	2-10		2-5		20-40	40-60			
1H 2879	877.5	15-30	10-20	5-15	5-15		20-40	20-40	2-10		
1H 2919	889.7		5-15		20-40		15-30	20-40			
1H 2946	897.9	2-10	2-10				30-50	30-50	2-10		
1H 2953	900.1	2-10	2-10				30-50	30-50	2-10		
1H 2988	910.7	5-15	5-15	Tr.			30-50	30-50	2-5		
1H 3050	929.6	5-15	5-15	2-5			20-40	40-60	2-10		
1H 3092	942.4	2-10	5-10	Tr.			40-60	30-50	2-5		
1H 3092(F)	942.4		2-10				30-50	20-40	15-30		
1H 3095	943.4	<5	5-15				30-50	40-60			
1H 3098	944.3	5-15	5-15				20-40	40-60	2-5		
1H 3128	953.4	5-15	5-15				20-40	40-60	2-5		
1H 3128(F)	953.4	2-5	2-5				20-40	20-40	15-30		
1H 3163	964.1	2-5	5-15				20-40	40-60	2-5		
1H 3163(F)	964.1		2-5				10-30	10-30	50-70		
1H 3185	970.8	10-25	10-20				20-40	30-50			
1H 3185(F)	970.8	<5	<5				5-15		60-80		2-10[b], 10-30[c]
1H 3196	974.1	2-10	5-15				20-40	40-60			
1H 3222	982.1	2-5	5-15				20-40	50-70			
1H 3225	983.0	5-15	5-15				20-40	40-60			
1H 3257	992.7	30-50	5-15				10-30	20-40			

TABLE XXXIII (Cont)

X-RAY DIFFRACTION ANALYSES OF TUFF FROM DRILL HOLE UE25B-1H (WEIGHT PERCENT)

Sample	Depth (m)	Smec-tite	Mica	Clino-ptilolite	Morden-ite	Anal-cime	Quartz	Alkali Feldspar	Calcite	Kaolinite	Other
1H 3267	995.8	15-30	2-10				30-50	20-40			
1H 3298	1005.2	5-15	2-10			Tr.	20-40	40-60			
1H 3326	1013.8	5-15	5-15			2-5	20-40	40-60			
1H 3362	1024.7	10-25	5-15			2-5	20-40	30-50		Tr.	
1H 3374	1028.4	5-15	5-15			10-30	20-40	20-40		<2	
1H 3393	1034.2	5-15	5-10			10-30	20-40	20-40	5-15	2-5	
1H 3401	1036.6	2-5	2-10			10-30	20-40	20-40	2-5	2-5	
1H 3459	1054.3	5-15	5-15			10-30	20-40	15-30	2-10	2-10	
1H 3469	1057.4	5-15	5-15			10-30	20-40	20-40	2-10	2-10	
1H 3506	1068.6	10-25	5-15			10-30	20-40	20-40	2-10	2-10	
1H 3530	1075.9	10-20	5-10			15-30	20-40	30-50	<5	<2	
1H 3530(F)	1075.9	10-20				5-15	20-40	20-40		5-10	
1H 3548	1081.4	5-15	5-15			2-5	20-40	30-50	2-10	2-5	
1H 3548(I)	1081.4	10-20	5-15				15-30	30-50	10-20	<2	
1H 3571	1088.4	5-10	2-10			2-5	30-50	15-30	20-40	<5	
1H 3572	1088.7	2-10	2-10			<2	20-40	30-50	15-30	<2	
1H 3572(I)	1088.7	10-25	5-15				20-40	20-40	5-15	<2	
1H 3602	1097.9	5-15	2-10			10-30	20-40	20-40	5-15	<2	
1H 3602(F)	1097.9	<5				5-15	2-10		30-50		30-50[b]
1H 3660	1115.6	5-15	2-10			15-30	20-40	20-40	2-10	2-5	
1H 3660(F)	1115.6					15-30	10-20	2-10	50-70		
1H 3708	1130.2	5-15	2-10				25-45	40-60		2-5	

TABLE XXXIII (Cont)

X-RAY DIFFRACTION ANALYSES OF TUFF FROM DRILL HOLE UE25B-1H (WEIGHT PERCENT)

Sample	Depth (m)	Smec-tite	Mica	Clino-ptilolite	Morden-ite	Anal-cime	Quartz	Alkali Feldspar	Calcite	Kaolinite	Other
1H 3767	1148.2	5-15	5-15			15-30	25-45	15-30	5-15	2-10	
1H 3792	1155.8	10-20	5-10			5-15	20-40	30-50	2-10	2-5	
1H 3835	1168.9	10-20	5-10			15-30	20-40	20-40	2-10	2-5	
1H 3880	1182.6	10-20	5-10			10-20	20-40	20-40	5-15	2-5	
1H 3901	1189.0	30-50	2-10			Tr.	20-40	15-30		Tr.	
1H 3902	1189.3	30-50	2-5		2-10		15-30	15-30	15-30		
1H 3904	1189.9	20-40				15-30	20-40	15-30	2-5		

[a]F = Fracture; S = Spherulite.

[b]Tridymite.

[c]Glass.

[d]Hematite.

[e]Kaolinite.

[f]Chlorite.

Clay minerals are almost ubiquitous throughout USW-G2, as in other drill cores of Yucca Mountain. Swelling clays (smectites) are present in most samples but are generally scarce in the bedded tuff of Calico Hills. The swelling capacities of the smectites undergo a transition at 3500 ft, where they pass from Na,Ca-saturation to K-saturation with a concomitant collapse and decrease of swelling capability. Kaolinites appear below 3500 ft in USW-G1 (3362 ft in UE25b-1H), and chlorite appears below 5500 ft in USW-G2 (UE25b-1H extends only to 4000 ft).

Several fractures were examined in detail for the study of UE25b-1H. The fractures are of interest because they provided pathways for element movement in the geologic past. Fractures may also provide pathways for future waste element movement, particularly if the fractures are not completely sealed. The fractures in UE25b-1H commonly contain calcite, in addition to the minerals in the fracture matrix. However, two fractures contain fluorite in substantial amounts. Also, a fracture with a brown band cutting the calcite contained todorokite, a manganese oxide hydrate common in marine deposits.

VI. VOLCANISM STUDIES (B. M. Crowe, D. T. Vaniman, F. V. Perry, and W. S. Baldridge).

A talk on "Strombolian Eruptive Sequences" was presented at the fall meeting of the American Geophysical Union. Data presented in the talk suggest a relatively low rate of magma rise (0.1 to 0.5 m s^{-1}, bubble free regime) for Quaternary basalt eruption in the NTS region. Eruptive sequences preserved in the NTS region can be explained by variations in the mass eruption rate with time and, therefore, by the history of bubble coalescence from the time of bubble exsolution to magma fragmentation. Low magma rise rates inferred for the basaltic rocks of the NTS allow more complete bubble coalescence, and thus more of the total volume of magma is erupted with the pyroclastic component.

A draft of a report, "Calculation of the Probability of Volcanic Disruption of a High-Level Radioactive Waste Repository within the Nevada Test Site Region, USA," has been completed. It will receive final editing early in the next quarter and be submitted to the NNWSI to fulfill a program milestone. The report develops a probability model (Pr) for the occurrence of a volcanic disruptive event. This can be formulated as

$$\Pr[\text{no disruptive event before time } t] = e^{-\lambda t p} \quad ,$$

where λ is a rate of volcanism and p is the probability of a disruptive event. The probability of a disruptive event (p) is a/A, where a is the area of a repository (for basaltic volcanism in the NTS region) and A is some minimal area that encloses the repository and the volcanic events used to describe λ. We have developed a computer program for determining A based on the distribution of volcanic centers in the NTS region. The parameter λ can be determined by two procedures, either rate of magma production with time, or counts of volcanic events over time (scoria cone counts).

Final revisions of a paper on "Aspects of Potential Magmatic Disruption of a High-Level Radioactive Waste Repository, Nevada Test Site" have been completed. The paper will be submitted to an outside journal for publication. Several new sources of data have been added to the paper. Final lithic fragment abundance calculations have been completed for scoria cones of the NTS region and the San Francisco Volcanic Field. The results are summarized in Table XXXIV. Literature surveys and field studies were completed to establish cone: sheet ratios of Strombolian eruptive centers. A conservative ratio of 4.5:1 was assigned for disruptive scenarios. Using this ratio, the magmatic volumes of all Quaternary basalt centers of the NTS region have been calculated (Table XXXV). Finally, thin-section studies have been completed of lithic

TABLE XXXIV

MEASUREMENTS OF LITHIC FRAGMENT ABUNDANCE IN STROMBOLIAN SCORIA CONES

Locality	Type[a]	% by Area	Correction	% by Volume
Lathrop Wells	A	0.013	--	0.009
Lathrop Wells	B	0.33	0.10	0.022
Lathrop Wells	A	0.048	--	0.032
Lathrop Wells	A	0.057	--	0.038
San Francisco Field	B	0.45	0.20	0.060
				Mean = 0.032 ± 0.019

[a]Type A measurements represent localities where the distribution of lithic fragments is relatively uniform throughout cone scoria. Type B localities are areas of lithic rich and lithic poor scoria. These measurements are corrected by the estimated percentage of lithic rich beds to the total scoria exposures.

TABLE XXXV

SIZE PARAMETERS FOR THE BASALTIC CENTERS OF THE NTS REGION

Volcanic Center	H(m)	W(m)	Cone Volume(m^3)	Flow Volume(m^3)	Vents	Total Magmatic Volume(m^3)[a]
Lathrop Wells	140	690	1.7×10^7	1.6×10^7	3	5.7×10^7
Little Cone #1	43	360	1.5×10^6	3.0×10^6	1	6.2×10^6
Little Cone #2	27	220	3.4×10^5	-	1	7.8×10^5
Red Cone	73	435	3.7×10^6	1.9×10^7	6	2.6×10^7
Black Cone	121	525	2.7×10^7	4.4×10^7	3	1.0×10^8
Sleeping Cone #1	63	240	2.7×10^6	4.9×10^6	1	1.1×10^7
Sleeping Cone #2	70	562	5.8×10^6	8.1×10^6	1	2.1×10^7

[a]Magmatic volume is equal to the volume of the cone plus the volume of an inferred scoria sheet, with the lava volume corrected to magmatic density.

fragments in cone scoria. These data indicate a relatively shallow depth of derivation (<200 m) of fragments, indicating incorporation during magma fragmentation (the point at which the bubble/magma ratio reaches 0.75).

VII. ROCK PHYSICS STUDIES (J. D. Blacic, J. Carter, P. M. Halleck, P. Johnson, T. J. Shankland, R. Anderson, and K. C. Spicochi)

A review has been completed that covers the likelihood of creep failure in rock types that might be selected for a high-level nuclear waste repository. This review will appear in the Proceedings of the Workshop on Near-Field Phenomena in Geologic Repositories for Radioactive Waste, under the title "Importance of Creep Failure of Hard Rock in the Near Field of a Nuclear Waste Repository." Although damage resulting from slow creep deformation may seem unlikely for a hard rock, experiments and models indicate that time-dependent microcracking and water-induced stress corrosion can lead to significant reductions in rock strength. Model extrapolations under dry conditions at 20 MPa confining pressure suggest small failure zones in the rib of the model repository room in hard rock during the first few years of operation. However, at 30 to 100 yr the modeled failure zone grows dramatically to completely encompass the near field of the room. Such a situation would be likely to block access to the repository.

Failure problems may be exacerbated under hydrous conditions. Extrapolations from existing experimental data suggest a 30 to 50% reduction in the compressive strength of granite over the 100-yr range critical to a repository, under water-saturated conditions. This estimate is based on extrapolations; the data for tuff are even less complete but suggest weakening comparable to that in water-saturated granite.

The review concludes that, contrary to intuition, creep deformation will occur under nuclear waste repository conditions. This deformation needs to be taken into consideration when designing repositories. Coupled phenomena make this conclusion even stronger. For instance, dilatant microcracking can cause a decrease in thermal conductivity leading to higher rock temperatures than those predicted by current models. A thorough laboratory investigation of hard rock creep deformation, particularly in tuff-based repository conditions, must be developed.

VIII. EXPLORATORY SHAFT

A. Design (D. C. Nelson, T. J. Merson, P. L. McGuire, J. W. Neudecker, and W. L. Sibbitt)

The draft, "Conceptual Design Report for the Exploratory Shaft (ES)," was completed on schedule. This report will be updated and issued after appropriate policy review.

A preliminary study evaluating the advantages and disadvantages of mining or drilling the ES shows that either technique is a viable option, and a final decision probably will not be made until the shaft depth has been selected.

Assuming that the ES is drilled, procurement orders must be placed for two items this fiscal year if the purchase option is to be exercised rather than leasing these items or using NTS equipment. These two items are a drill rig (about $6 million), with an 18-month delivery time, and the power casing tongs (about $110 000), with a 12-month delivery time. Currently, no capital equipment funds are authorized in FY-1982 for these items.

Assistance has been provided in scoping a surface excavation to evaluate the unsaturated zone rather than drill a vertical borehole. One approach would be to construct an adit into a Topopah Spring outcropping where various in situ experiments can be conducted.

B. Experiment Test Plan (C. W. Myers, D. C. Nelson, and B. R. Erdal)

The objective of this task is to develop an experiment test plan that will assess the in situ thermomechanical, hydrologic/geochemical, and geologic characteristic of a tuffaceous target horizon in Yucca Mountain to determine its suitability for a Test and Evaluation Facility (TEF) and a repository. The planning for this activity has been initiated.

The test plan is to be developed according to the following guidelines. 1) Development of the test plan is to be a joint endeavor with active participation from appropriate NNWSI organizations and with invited participation from other organizations as needed. Development of the data requirements should not be limited to those areas of investigation in which a given organization is currently involved in NNWSI. 2) Development of the test plan should benefit and draw heavily from experience gained elsewhere in the NWTS program. Specifically, the test plans for basalt and salt should be utilized extensively, and the format for the tuff test plan document should parallel those documents as appropriate to facilitate comparisons of the test plan. 3) Los Alamos is

responsible for planning and coordinating the development of the test plan. This includes scheduling and controlling delivery of individual topics and subtopics to be included in the test plan, as well as compilation and completion of the draft test plan. 4) The draft test plan should be subjected to extensive internal NNWSI review. External review of the tuff test plan should include comment by BWIP (basalt) and ONWI (salt) reviewers knowledgeable of their respective test plans.

In developing the ES test plan, we will first define the data required for each step of the exploration (see below). Ranges of acceptable and unacceptable results must be identified, and criteria and methods by which suitability is to be judged must be defined. A ranking or priority will be assigned to each set of required data. This will place greatest emphasis on the most needed data sets. Only after the above data sets have been identified can the tests be selected to obtain the required data.

The testing program will proceed in a series of steps; each subsequent step is dependent upon favorable results obtained from the previous series of tests. As currently defined, the test plan will include the following exploration steps: Step 1) Confirmatory borehole; Step 2) Phase I (TEF site verification) during shaft construction or in completed shaft; Step 3) Phase I (TEF site verification) for characterization of horizon of interest; Step 4) Phase II (repository site verification); and Step 5) At-depth testing (repository design verification).

IX. QUALITY ASSURANCE (P. L. Bussolini, R. R. Geoffrion, J. J. Simpson, and R. J. Romero)

A. Los Alamos National Laboratory

The Los Alamos NNWSI Organization Chart and the Quality Assurance Program Plan were revised, but approvals have not yet been secured. Personnel certifications for Earth & Space Sciences (ESS) Division were prepared and put on file. Chemistry-Nuclear Chemistry (CNC) Division personnel certifications were prepared and are being approved. An indoctrination and training session for new project personnel is being developed.

The Sorption Coefficient and Migration Measurements Work Plan was revised. The revision completes the July audit by DOE.

The Exploratory Shaft Work Plan is being revised, and three design procedures were written for the exploratory shaft work.

B. US Geological Survey

Procedure NWM-USGS-MDP-1, The Identification, Handling, Storage, and Disposition of Drill Hole Core and Samples, was approved and distributed. The Gravity Measurements and Data Reduction Procedure, NWM-USGS-GPP-01, was revised by Menlo Park personnel and approvals are being obtained. Approval signatures were secured on six hydrology procedures and on a heat flow geophysics procedure. A Unit Task Procedure for the geologic investigations was drafted.

X. PUBLICATIONS AND ABSTRACTS

1. R. S. Rundberg, S. Maestas, and J. L. Thompson, "Radionuclide Migration: Laboratory Experiments with Isolated Fractures," International Symposium on the Scientific Basis for Nuclear Waste Management, Materials Research Society, Boston, Massachusetts, November 16, 1981.

2. B. R. Erdal, R. S. Rundberg, K. Wolfsberg (Los Alamos National Laboratory); D. L. Fortney, K. L. Erickson (Sandia National Laboratories); A. M. Friedman, S. Fried, and J. J. Hines (Argonne National Laboratory, "Nuclide Migration Field Experiments in Tuff, G Tunnel, Nevada Test Site," International Symposium on the Scientific Basis for Nuclear Waste Management, Materials Research Society, Boston, Massachusetts, November 16, 1981.

3. B. Crowe, S. Self, and R. C. Amos, "Strombolian Eruptive Sequences," Am. Geophys. Union Fall Meeting, San Francisco, California, December 8, 1981.

4. R. C. Amos, S. Self, and B. Crowe, "Pyroclastic Activity of Sunset Crater: Evidence for a Large Magnitude, High Disposal Strombolian Eruption," Am. Geophys. Union Fall Meeting, San Francisco, California, December 8, 1981.

5. J. D. Blacic, "Importance of Creep Failure of Hard Rock in the Near Field of a Nuclear Waste Repository," Workshop on Near-Field Phenomena in Geologic Repositories for Radioactive Waste, Seattle, Washington, August 31 - September 3, 1981 (in press).

6. D. C. Nelson, T. J. Merson, W. L. Sibbitt, and P. L. McGuire, "Conceptual Design Report, Exploratory Shaft, Nevada Nuclear Waste Storage Investigations," Los Alamos National Laboratory report LA-9179-MS (1982, in press).

7. J. D. Blacic, "Importance of Time-Dependent Deformation of Hard Rocks in the Near Field of a Nuclear Waste Repository," OECD/NEA Workshop on Near-Field Phenomena in Geologic Repositories for Radioactive Waste, Seattle, Washington, August 31 - September 3, 1981 (in press).

8. D. Vaniman and D. Bish, "Zeolite and Clay Mineral Stability at Yucca Mountain, Nevada," NWTS Information Meeting, Columbus, Ohio, November 19, 1981 (Abstract).

9. D. T. Vaniman and B. M. Crowe, "Trace Element Enrichments in Late Cenozoic Basaltic Volcanism of the Southcentral Great Basin, Nevada and California," Geological Society of America, March 1982 (Abstract).

10. D. L. Bish, "Smectite and Zeolite Distributions and Reactions in Tuffs at Yucca Mountain," American Chemical Society, Las Vegas, Nevada, March 1982 (Abstract).

11. R. S. Rundberg, S. J. Knight, and J. L. Thompson, "Sorption Isotherms and Matrix Diffusion in Yucca Mountain Tuff," American Chemical Society, Las Vegas, Nevada, March 1982 (Abstract).

12 F. Caporuscio, D. Vaniman, D. Bish, D. Broxton, B. Arney, G. Heiken, F. Byers, R. Gooley, and R. Semarge, "Petrologic Studies of Drill Hole USW-G2 and of the Lower Crater Flat Tuff in Drill Hole UE25b-1H, Yucca Mountain, Nevada," Los Alamos National Laboratory report LA-9255-MS (in press, 1982).

ACKNOWLEDGMENTS

The following Los Alamos National Laboratory personnel are acknowledged for the efforts mentioned: D. A. Mann (technical assistance), P. A. Elder, M. E. Lark, and S. Lermuseaux (sample counting and gamma-spectral analyses), and L. M. Mitchell and C. E. Gallegos (typing of drafts and final manuscript).

REFERENCES

1. W. R. Daniels, K. Wolfsberg, D. T. Vaniman, and B. R. Erdal, Eds., "Research and Development Related to Nevada Nuclear Waste Storage Investigations, July 1 - September 30, 1981," Los Alamos National Laboratory report LA-9095-PR (January 1982).

2. K. Wolfsberg, B. P. Bayhurst, B. M. Crowe, W. R. Daniels, B. R. Erdal, F. O. Lawrence, A. E. Norris, and J. R. Smyth, "Sorption-Desorption Studies on Tuff. I. Initial Studies with Samples from the J-13 Drill Site, Jackass Flats, Nevada," Los Alamos Scientific Laboratory report LA-7480-MS (April 1979).

3. R. W. Weast, Ed., Handbook for Chemistry and Physics, 55th Ed. (CRC Press, Cleveland, 1975), p. C-185.

4. E. W. Martin and E. F. Cook, Eds, Remington's Practice of Pharmacy (Hack, Easton, Pennsylvania, 1961), p. 1143.

5. K. Wolfsberg and E. N. Vine,"Correlation of Sorptive Properties of Tuff Water Mineralogy," in "Evaluation of Tuff on a Medium for a Nuclear Waste Repository: Interim Status Report on the Properties of Tuff," J. K. Johnstone and K. Wolfsberg, Eds., Sandia National Laboratories report SAND80-1464 (July 1980).

6. E. N. Vine, R. D. Aguilar, B. P. Bayhurst, W. R. Daniels, S. J. DeVilliers, B. R. Erdal, F. O. Lawrence, S. Maestas, P. Q. Oliver, J. L. Thompson, and K. Wolfsberg, "Sorption-Desorption Studies on Tuff. II. A Continuation of Studies with Samples from Jackass Flats, Nevada, and Initial Studies with

Samples from Yucca Mountain, Nevada," Los Alamos Scientific Laboratory report LA-8110-MS (January 1980).

7. D. Langmuir, "Uranium Solution-Mineral Equilibria at Low Temperatures with Applications to Sedimentary Ore Deposits," Geochim. Cosmochim. Acta. 42, 547 (1978).

8. B. R. Erdal, W. R. Daniels, D. T. Vaniman, and K. Wolfsberg, Eds., "Research and Development Related to the Nevada Nuclear Waste Storage Investigations, April 1 - June 30, 1981," Los Alamos National Laboratory report LA-8959-PR (October 1981).

9. B. R. Erdal, R. D. Aguilar, B. P. Bayhurst, W. R. Daniels, C. J. Duffy, F. O. Lawrence, S. Maestas, P. Q. Oliver, and K. Wolfsberg, "Sorption-Desorption Studies on Granite. I. Initial Studies of Strontium, Technetium, Cesium, Barium, Cerium, Europium, Uranium, Plutonium, and Americium," Los Alamos Scientific Laboratory report LA-7456-MS (February 1979).

10. B. R. Erdal, Ed., "Laboratory Studies of Radionuclide Distributions Between Selected Groundwaters and Geologic Media, Annual Report, October 1, 1978 - September 30, 1979," Los Alamos Scientific Laboratory report LA-8088-PR (February 1980).

11. B. R. Erdal, W. R. Daniels, and K. Wolfsberg, Eds., "Research and Development Related to Nevada Nuclear Waste Storage Investigations, January 1 - March 31, 1981," Los Alamos National Laboratory report LA-8847-PR (July 1981).

12. K. Wolfsberg, R. D. Aguilar, B. P. Bayhurst, W. R. Daniels, S. J. DeVilliers, B. R. Erdal, F. O. Lawrence, S. Maestas, A. J. Mitchell, P. Q. Oliver, N. A. Raybold, R. S. Rundberg, J. L. Thompson, and E. N. Vine, "Sorption-Desorption Studies on Tuff. III. A Continuation of Studies with Samples from Jackass Flats and Yucca Mountain, Nevada," Los Alamos National Laboratory report LA-8747-MS (May 1981).

13. K. Wolfsberg and B. R. Erdal, Eds., "Research and Development Related to the Nevada Nuclear Waste Storage Investigations, October 1 - December 31, 1980," Los Alamos National Laboratory report LA-8739-PR (April 1981).

14. G. W. Thomas and A. R. Swoboda, "Anion Exclusion Effects on Chloride Movement in Soils," Soil Sci. 110, 163-166 (1970).

15. D. K. Cassel, M. Th. VanGrenuchten, and P. J. Wierenga, "Predicting Anion Movement in Disturbed and Undisturbed Soils," Soil Sci. Soc. Am. Proc. 39, 1015 (1975).

16. I. Neretnieks, "Diffusion in the Rock Matrix: An Important Factor in Radionuclide Retardation?" J. Geophys. Res. 85, 4379 (1980).

17. K. L. Erickson and D. R. Fortney, "Preliminary Transport Analyses for Design of the Tuff Radionuclide Migration Field Experiment," Sandia National Laboratories report SAND81-1253 (September 1981).

18. J. Crank, The Mathematics of Diffusion, 2nd Ed. (Oxford University Press, London, 1975), p. 52.

19. G. E. Manger, "The Best Value of Porosity of Lapilli Tuff from the Nevada Test Site," US Geol. Surv. Prof. Paper 525-B, B146-B150 (1965).

20. L. K. Porter, W. D. Kemper, R. D. Jackson, and B. C. Stewart, "Chloride Diffusion in Soils as Influenced by Moisture Content," Soil Sci. Soc. Am. Proc. 24, 460-463 (1960).

21. J. Kielland, "Individual Activity Coefficients of Ions in Aqueous Solutions," J. Am. Chem. Soc. 59, 1675 (1937).

22. R. W. Weast, Ed., Handbook of Chemistry and Physics, 62nd Ed. (Chemical Rubber Publishing Co., Boca Raton, Florida, 1981), p. D-142.

23. R. Kuhn and A. Wasserman, "Die Dissoziationskonstanten der Halogenbenzoesauren," Helv. Chim. Acta 11, 31 (1928).

24. M. T. Ryan and K. J. Berner, "Λ_{OH} and pKa Values of Para Substituted Tetrafluorobenzoic Acids," Spectrochim. Acta 25A, 1155 (1969).

25. P. A. Witherspoon, J. S. Y. Wang, K. Iwai, and J. E. Gale, "Validity of Cubic Law for Fluid Flow in a Deformable Rock Fracture," Lawrence Berkeley Laboratory report LBL-9557 (October 1979).

26. M. H. Lloyd and R. G. Haire, "The Chemistry of Plutonium in Sol-Gel Processes," Radiochim. Acta 25, 139 (1978).

27. D. Rai and J. L. Swanson, "Properties of Plutonium (IV) Polymer of Environmental Importance," Nucl. Technol. 54, 107 (1981).

28. J. B. Andelman and T. C. Rozzell, "Plutonium in the Water Environment," in Radionuclides in the Environment, Advances in Chemistry Series 93, R. F. Gould, Ed. (American Chemical Society, Washington, D. C. 1970), pp. 118-137.

29. J. J. Katz and G. T. Seaborg, The Chemistry of the Actinide Elements (Methuen and Co., Ltd., London, 1957), p. 300 and refs. cited.

30. D. A. Costanzo, R. E. Biggers, and J. T. Bell, "Plutonium Polymerization," J. Inorg. Nucl. Chem. 35, 609 (1973).

31. S. W. Rabideau, "The Kinetics of the Disproportionation of Plutonium (V)," J. Am. Chem. Soc. 79, 6350 (1957).

32. B. Allard, H. Kipatsi, and J. O. Liljenzin, "Expected Species of Uranium, Neptunium, and Plutonium in Neutral Aqueous Solutions," J. Inorg. Nucl. Chem. 42, 1015 (1980).

33. M. L. Sykes, G. H. Heiken, and J. R. Smyth, "Mineralogy and Petrology of Tuff Units from the UE25a-1 Drill Site, Yucca Mountain, Nevada," Los Alamos Scientific Laboratory report LA-8139-MS (November 1979).

34. J. R. Smyth and F. A. Caporuscio, "Review of the Thermal Stability and Cation Exchange Properties of the Zeolite Minerals Clinoptilolite, Mordenite, and Analcime: Applications to Radioactive Waste Isolation in Silicic Tuff," Los Alamos National Laboratory report LA-8841-MS (June 1981).

APPENDIX

FREE ENERGY OF FORMATION OF SOME MINERALS IN NEVADA TUFF

J. F. Kerrisk

I. INTRODUCTION

As part of the Nevada Nuclear Waste Storage Investigation, the chemistry of groundwater in the vicinity of Yucca Mountain is being studied. One aspect of these studies is the development of chemical-equilibrium models for the interaction of groundwater with minerals in the local tuff. To model these systems, thermodynamic data in the form of equilibrium constants or free energies of formation for the local minerals are required. Some of these data are available in thermodynamic data bases or as part of existing computer programs that model chemical equilibrium. Data for other minerals, such as some of the zeolites found near Yucca Mountain, have not been measured.

This appendix describes the results of a preliminary search for free-energy data at 25°C for some of the mineral phases found during exploratory drilling at or near Yucca Mountain. The reactions of primary interest are the formation of the minerals from aqueous species. Equilibrium-constant or free-energy data are presented for these formation reactions from a particular basis set of aqueous species. Data were found for silica (crystalline and amorphous forms), alkali feldspars, some clays, and one zeolite (analcime). No data were found for three other zeolites observed at Yucca Mountain: clinoptilolite, heulandite, and mordenite. Free-energy data were estimated for these minerals by three different techniques. Many of the minerals of interest actually exist as solid solutions; however, few thermodynamic data are available for solid solutions. The data presented here are all for simple compounds with specific compositions.

II. MINERALS OF INTEREST

Exploratory drilling in the vicinity of Yucca Mountain has sampled areas of interest for radioactive-waste storage.[1-3] These areas are primarily beds of silicic tuffs, which contain large amounts of zeolites.[3] Table A-I lists minerals that have been observed in and near these beds. The tuff also contains varying amounts of vitreous material or glass. This glass is not a thermodynamically stable phase; it cannot be assigned thermodynamic data or employed in equilibrium calculations.

Analyses of mineral phases generally yield a range of compositions.[1,2] For chemical modeling, however, specific compositions are usually needed.* Table A-I also includes chemical formulae that were used to develop the thermodynamic data. The silica minerals all have the formula SiO_2. Amorphous

---

*If a chemical equilibrium model considers solid solutions, the solid-solution phase has a variable composition. Only one computer model, EQ3/6, has begun to introduce solid solutions, but that work has not been completed.

TABLE A-I

MINERALS OF INTEREST IN THE YUCCA MOUNTAIN AREA

Group	Mineral	Chemical Formula[a]
Silica	Quartz	SiO_2
	Cristobalite	SiO_2
	Amorphous silica	SiO_2
Alkali feldspar	Albite	$NaAlSi_3O_8$
	Sanidine	$KAlSi_3O_8$
	Microcline	$KAlSi_3O_8$
Clay	Montmorillonite	Varies
	Beidellite	$XAl_7Si_{11}O_{30}(OH)_6$
	Beidellite	$ZAl_{14}Si_{22}O_{60}(OH)_{12}$
	Nontronite	$XAlFe_6Si_{11}O_{30}(OH)_6$
	Nontronite	$ZAl_2Fe_{12}Si_{22}O_{60}(OH)_{12}$
Zeolite	Analcime	$Na[AlSi_2O_6]\cdot H_2O$
	Clinoptilolite	$X_2[Al_2Si_{10}O_{24}]\cdot 8H_2O$
	Clinoptilolite	$Z[Al_2Si_{10}O_{24}]\cdot 8H_2O$
	Heulandite	$Ca[Al_2Si_7O_{18}]\cdot 6H_2O$
	Mordenite	$X[AlSi_5O_{12}]\cdot 3H_2O$

[a]X = Na or K; Z = Ca or Mg.

silica may actually be hydrated, but it is usually treated as SiO_2 in equilibrium calculations. Sanidine ($KAlSi_3O_8$) and albite ($NaAlSi_3O_8$) are two alkali feldspars found at Yucca Mountain for which thermodynamic data are available. The Si/Al atomic ratios measured for the phases identified as alkali feldspars generally range from 3 to 3.4 (Ref. 2). These phases may contain some silica, so the formulae noted above are probably representative (see Table A-I). All of the alkali feldspars observed have both sodium and potassium present.[1,2] They are probably solid solutions rather than mixtures of pure compounds. Thus, modeling only the pure compounds is an approximation to the actual situation. Polymorphs (minerals with the same chemical formula, but different structures) of sanidine and albite have also been observed at Yucca Mountain.[2] Although free-energy data for reactions involving polymorphs are generally similar, significant differences can exist.[4] Data for microcline, a polymorph of sanidine, are included here for comparison.

Clay identified as montmorillonite has been observed in the Yucca Mountain area.[1,2] Table A-II lists some atomic ratios for a few of the samples. Montmorillonite is one of the smectite group of clays.[5] Thermodynamic data were found for a number of smectite clays with the montmorillonite structure (see Table A-I). The formulae labeled beidellite in Table A-I have been called montmorillonite in chemical literature.[6] The observed Si/Al and Si/Fe atomic ratios (see Table A-II) do not match either the beidellite or nontronite formulae in Table A-I. They appear to represent some intermediate material. Thermodynamic data are also available for a number of true montmorillonite clays with specific alkali metal and alkaline earth compositions; they include clays such as Aberdeen, Belle Fourche, Colony, Arizona, and Wyoming montmorillonites. Some data are presented for these materials. The alkali metal and alkaline earth cations in clays are thought to occupy easily exchanged positions. The actual minerals are more nearly solid solutions, where all the cations may be present. As with the alkali feldspars, the thermodynamic data are for compounds with specific compositions.

Four zeolites have been identified in the Yucca Mountain area; they are analcime, clinoptilolite, heulandite, and mordenite. Table A-III lists some atomic ratios for a few of the samples of these minerals. Zeolites usually show a range of compositions. The formulae for these minerals listed in Table A-I are generally accepted.[7-9] The predominant cation observed for analcime is sodium.[1] The single formula in Table A-I represents the observed composition of analcime reasonably well. Clinoptilolite shows varying amounts of sodium, potassium, calcium, and magnesium.[1,2] These cations are normally exchangeable; thermodynamically, the mineral should probably be considered as a solid solution. Only the four pure compounds shown in Table A-I were considered. Heulandite is structurally similar to clinoptilolite; the Si/(Al+Fe) ratio is lower and the exchange cation is predominantly calcium.[1,2] The single formula in Table A-I represents the observed composition. Mordenite shows predominantly sodium and potassium as the exchange cations.[2] The

TABLE A-II

MONTMORILLONITE DATA FROM YUCCA MOUNTAIN AREA

Sample	Atomic Ratios		
	Si/Al	Si/Fe	Alkaline Earth/ Alkali Metal
UE25a-1[a]			
YM-43	4.7	28	0.003
YM-45	3.1	94	0.088
YM-53	3.5	49	0.028
J-13[b]			
JA-36-BC	3.1	41	0.40
JA-36-BC	2.4	47	0.55

[a]Reference 2.
[b]Reference 1.

TABLE A-III

ZEOLITE DATA FROM YUCCA MOUNTAIN AREA

Mineral	Sample	Si/Al+Fe	Fe/Al	Alkaline Earth/ Alkali Metal
Analcime	J-13[a]			
	JA-26	2.9	<0.01	0.005
	JA-31	2.7	<0.01	0.007
	JA-35	2.3	<0.01	0.003
Clinoptilolite	UE25a-1[b]			
	YM-32	5.2	<0.01	1.61
	YM-35	6.1	<0.01	0.81
	YM-36	5.1	<0.01	1.43
	YM-38	4.4	<0.01	0.85
	YM-40	4.8	0.04	0.70
	YM-47	5.5	<0.01	1.09
	YM-49	5.7	0.05	0.42
	YM-51	5.0	<0.01	1.62
	J-13[a]			
	JA-20	4.6	NR[c]	1.49
	JA-23	4.7	<0.01	1.23
Heulandite	UE25a-1[b]			
	YM-30	3.9	<0.01	8.5
	YM-31	3.2	0.04	3.1
	YM-42	3.8	<0.01	3.7
	YM-42	4.2	<0.01	1.5
Mordenite	UE25a-1[b]			
	YM-46	3.2	<0.01	0.008
	YM-46	3.0	0.15	0.009

[a]Reference 1.
[b]Reference 2.
[c]NR = not reported.

observed Si/(Al+Fe) ratios (see Table A-III) are somewhat below the accepted formulae for mordenite (see Table A-I). Free-energy data were found for analcime only. Data were estimated for clinoptilolite, heulandite, and mordenite by three different techniques.

III. DATA FROM EXISTING SOURCES

There are many existing compilations of free-energy or equilibrium-constant data that include information on mineral species. Helgeson has produced a number of such compilations,[6] the most recent being the SUPCRT computer program.[10] The data collected by Robie and Waldbaum, which represent

free energies of formation of minerals from the elements in their standard states, are also widely used.[11] Recently, Benson and Teague have tabulated thermodynamic data of interest for radioactive waste systems.[12] Another source of data is the chemical-equilibrium computer programs that include thermodynamic data in their data bases. Four programs available at Los Alamos are EQ3/6,[13] WATEQF,[14] GEOCHEM,[15] and REDEQL.EPAK.[16] Data from WATEQ2[17] are also available, although the program is not currently running here.

In some cases, there is considerable disagreement among the various sources of data. Data from different sources are presented here to show the range of disagreement or uncertainty that exists. All data are presented as $\log_{10} K$, where K is the equilibrium constant for the formation reaction of the mineral from aqueous species at 25°C. The free energy for this reaction (ΔG°_r) is related to K as

$$\Delta G^{\circ}_r = -2.3026\ RT \log_{10} K \quad ,$$

where R is the gas constant (1.9872 cal/mole K) and T is the absolute temperature (K). At 25°C (T = 298.15 K),

$$\Delta G^{\circ}_r (\text{K cal/mole}) = -1.364 \log_{10} K \quad .$$

The formation reactions for the various minerals from the aqueous species are listed in the sections describing the data.

A. Silica

The formation reaction for solid silica phases is

$$SiO_2^{\circ} = SiO_2(x) \quad , \tag{1}$$

where SiO_2° is the aqueous silica species and x is q, c, or a for quartz, cristobalite, and amorphous silica, respectively. (Some data bases use $H_2SiO_3^{\circ}$ or $H_4SiO_4^{\circ}$ as the basic aqueous species.) Table A-IV lists values of $\log_{10} K$ for Eq. (1). It is evident that many of the compilations or data bases use the same source. The agreement among the various sources is quite good.

B. Alkali Feldspar

The formation reactions for the two alkali feldspars are

$$Na^+ + Al^{+3} + 3SiO_2^{\circ} + 2H_2O_l = NaAlSi_3O_8 + 4H^+ \text{ and} \tag{2}$$

$$K^+ + Al^{+3} + 3SiO_2^{\circ} + 2H_2O_l = KAlSi_3O_8 + 4H^+ \quad , \tag{3}$$

where H_2O_l is liquid water. Table A-V lists values of $\log_{10} K$ for these reactions. Three of the sources list data for low and high albite.[10,12,13] They are all based on SUPCRT. WATEQF lists data for albite only; it does not have data for sanidine or microcline, but the value for adularia ($KAlSi_3O_8$), a polymorph of sanidine, is shown for comparison. The agreement among the various sources is quite good.

TABLE A-IV

THERMODYNAMIC DATA FOR SILICA MINERALS

Source	$\log_{10} K^a$		
	$SiO_2(q)$	$SiO_2(c)$	$SiO_2(a)$
SUPCRT (Ref. 10)	+4.00	+3.45	+2.71
Benson and Teague (Ref. 12)	+4.00	+4.18	+2.71
WATEQF (Ref. 14)	+4.01	+3.59	+3.02
EQ3/6 (Ref. 13)	+4.00	+3.45	+2.71
REDEQL.EPAK (Ref. 16)	-	-	+2.70[b]
GEOCHEM (Ref. 15)	-	-	+2.70[b]

[a]$\log_{10}$ K for Eq. (1).
[b]Only one solid silica phase available in the program.

TABLE A-V

THERMODYNAMIC DATA FOR ALKALI FELDSPAR MINERALS

Source	$\log_{10}$ K		
	Albite Eq. (2)	Sanidine Eq. (3)	Microcline Eq. (3)
SUPCRT (Ref. 10)	-3.10[a] -4.42[b]	-1.28	-0.08
Benson and Teague (Ref. 12)	3.09[a] -4.41[b]	-1.25	-0.05
WATEQF (Ref. 14)	-4.05	-1.48[c]	-
EQ3/6 (Ref. 13)	-3.08[a] -4.40[b]	-1.37	-0.17

[a]Low albite.
[b]High albite.
[c]Data are for adularia; no sanidine data are available.

C. Clays

The formation reactions for the beidellite clays are

$$X^{+} + 7Al^{+3} + 11SiO_2^{\bullet} + 14H_2O_1 = XAl_7Si_{11}O_{30}(OH)_6 + 22H^{+} \text{ and} \quad (4)$$

$$Z^{+2} + 14Al^{+3} + 22SiO_2^{\bullet} + 28H_2O_1 = ZAl_{14}Si_{22}O_{60}(OH)_{12} + 44H^{+} \quad , \quad (5)$$

where X is Na or K, and Z is Ca or Mg. Table A-VI lists values of $\log_{10} K$ for these reactions. The data from GEOCHEM do not agree with data from other sources. The difference between WATEQF and WATEQ2 for Ca-beidellite is also puzzling.

The formation reactions for the nontronite clays are

$$X^{+} + Al^{+3} + 6Fe^{+3} + 11SiO_2^{\bullet} + 14H_2O_1 = XAlFe_6Si_{11}O_{30}(OH)_6 + 22H^{+} \quad (6)$$

and

$$Z^{+2} + 2Al^{+3} + 12Fe^{+3} + 22SiO_2^{\bullet} + 28H_2O_1 = ZAl_2Fe_{12}Si_{22}O_{60}(OH)_{12} + 44H^{+} \quad , \quad (7)$$

where X is Na or K, and Z is Ca or Mg. Table A-VII lists values of $\log_{10} K$ for these reactions. The data used in EQ3/6 have been estimated by Wolery.[13]

Free-energy data have been measured or estimated for a number of montmorillonite clays with specific compositions.[14,18-20] Except in a few isolated cases, these materials are not available in current chemical-equilibrium computer programs. Table A-VIII lists a sampling of the data. The quantity ΔG°_f is the free energy of formation of the mineral from the elements in their standard states at 25°C; in some cases, it is the only datum reported. For

TABLE A-VI

THERMODYNAMIC DATA FOR BEIDELLITE CLAYS

	$\log_{10} K$			
Source	X = Na Eq. (4)	X = K Eq. (4)	Z = Ca Eq. (5)	Z = Mg Eq. (5)
Helgeson (Ref. 6)	-19.06	-18.32	-37.10	-36.60
WATEQF (Ref. 14)	-	-	-38.7	-
WATEQ2 (Ref. 17)	-	-	-51.8	-
GEOCHEM (Ref. 15)	-11.7	-10.5	-21.6	-21.7
REDEQL.EPAK (Ref. 16)	-20.7	-	-	-
EQ3/6 (Ref. 13)	-19.12	-18.24	-38.02	-37.81

TABLE A-VII

THERMODYNAMIC DATA FOR NONTRONITE CLAYS

Source	$\log_{10}$ K			
	X = Na Eq. (6)	X = K Eq. (6)	Z = Ca Eq. (7)	Z = Mg Eq. (7)
EQ3/6 (Ref. 13)	+47.6	+48.4	+95.3	+95.6

these minerals, the equilibrium constant for formation from aqueous species (K) was calculated as described in Sec. IV, using data from SUPCRT.[10]

D. Zeolites

Thermodynamic data were found for only one zeolite that had been detected in the Yucca Mountain area -- analcime. The formation reaction for analcime is

$$Na^{+} + Al^{+3} + 2SiO_2^{\bullet} + 3H_2O_l = NaAlSi_2O_6 \cdot H_2O + 4H^{+} \quad . \qquad (8)$$

Table A-IX lists values of $\log_{10}$ K for this reaction. The later, more positive, value from SUPCRT and EQ3/6 results from a re-evaluation of the experimental data by Helgeson.[10] Data for other zeolites, not detected in the Yucca Mountain area, are also available.[10] Some of these data are discussed in Sec. IV.

IV. ESTIMATED DATA

Free-energy data for three zeolites observed in the Yucca Mountain area could not be found. They are clinoptilolite, heulandite, and mordenite. Three methods were used to estimate thermodynamic data for these minerals. Two of the methods were developed to estimate free energy of formation of clays.[18,19] They have not previously been applied to zeolites. The third method has had more general application.[4] In addition to the calculations for the three zeolites noted above, calculations were also done for three other zeolites (analcime, wairakite, and laumonite) for comparison with measured data.

All three methods estimate the free energy of formation of a mineral from the elements in their standard states at 25°C (ΔG°_f). For use in aqueous chemical-equilibrium calculations, the free energy (ΔG°_r) or equilibrium constant (K) for the formation reaction from aqueous species must be known. This requires a knowledge of values of ΔG°_f for the aqueous species. With these data, ΔG°_f for a mineral can be converted into ΔG°_r or K for that mineral. The values of ΔG°_f for the aqueous species should be consistent with the thermodynamic data employed to estimate ΔG°_f for that mineral. Values of ΔG°_f for aqueous species from three different sources were used in these calculations.[10,11,19] The data are shown in Table A-X. The only significant difference for the zeolite calculations is in ΔG°_f for Al^{+3}; the value used by Tardy and Garrels is 2 to 3 kcal/mole more negative than from the other sources.

TABLE A-VIII

THERMODYNAMIC DATA FOR MONTMORILLONITE CLAYS

Formula	ΔG°_f [a] (kcal/mole)	$\log_{10} K$ [b]	Source
$(H,Na,K)_{0.28}Mg_{0.29}Fe_{0.23}Al_{1.58}Si_{3.93}O_{10}(OH)_2$	-	+0.1	WATEQF (Ref. 14)
$(H,Na,K)_{0.42}Mg_{0.45}Fe_{0.34}Al_{1.47}Si_{3.82}O_{10}(OH)_2$	-	-2.6	WATEQF (Ref. 14)
$(Ca_{0.19}Na_{0.02}K_{0.02})[Mg_{0.33}Fe_{0.14}Al_{1.59}Si_{3.93}O_{10}](OH)_2$	-1252.1	-11.1	Nriagu (Ref. 18)
$(Ca_{0.1}Na_{0.27}K_{0.02})[Mg_{0.22}Fe_{0.19}Al_{1.58}Si_{3.94}O_{10}](OH)_2$	-1248.2	-7.8	Nriagu (Ref. 18)
$Mg_{0.225}[Mg_{0.27}Fe_{0.405}Al_{1.645}Si_{3.70}O_{10}](OH)_2$	-1246.3	+1.4	Mattigod and Sposito (Ref. 20)

[a] ΔG°_f is the free energy of formation from the elements in their standard states at 25°C.

[b] K is the equilibrium constant for formation of the mineral from aqueous species Na^+, K^+, H^+, Mg^{+2}, Ca^{+2}, Fe^{+3}, Al^{+3}, SiO_2°, and H_2O_l.

TABLE A-IX

THERMODYNAMIC DATA FOR ANALCIME

Source	$\log_{10} K$ Eq. (8)
SUPCRT (Ref. 10)	-7.28
Helgeson (Ref. 6)	-9.37
WATEQF (Ref. 14)[a]	-9.35
EQ3/6 (Ref. 13)	-7.26

[a]WATEQ2 (Ref. 17) uses the same value.

The following sections briefly describe the three methods of estimating ΔG°_f of the minerals and present the results.

A. Tardy and Garrels

Tardy and Garrels proposed a simple method of estimating ΔG°_f of layer silicates.[19] A reaction that forms the desired mineral is written in terms of the oxides of the elements involved. With analcime, for example,

$$\frac{1}{2}[Na_2O]_{ex} + \frac{1}{2}[Al_2O_3]_{sil} + 2[SiO_2]_{sil} + [H_2O]_{sil} = NaAlSi_2O_6 \cdot H_2O \quad , (9)$$

where the subscript ex implies that a free energy of formation associated with an exchange reaction should be used for the species, and the subscript sil

TABLE A-X

ΔG°_f FOR AQUEOUS SPECIES

Aqueous Species	ΔG°_f (kcal/mole) Tardy and Garrels (Ref. 19)	SUPCRT (Ref. 10)	Robie and Waldbaum (Ref. 11)
Na^+	-62.5	-62.62	-62.54
K^+	-67.7	-67.58	-67.70
Ca^{+2}	-132.2	-132.16	-132.18
Mg^{+2}	-108.9	-108.70	-108.90
Al^{+3}	-119.5	-116.97	-116.00
Fe^{+3}	-	-1.10	-2.52
SiO_2°	-199.12	-199.19	-199.18[a]
H_2O_l	-56.69	-56.69	-56.69
OH^-	-37.6	-37.60	-37.59
H^+	0	0	0

[a]Required ΔG°_r for $Si_2O^{\circ} + H_2O = H_2SiO_3^{\circ}$.
Taken as $\Delta G^{\circ}_r = -2.13$ kcal/mole from Ref. 12.

implies that a free energy of formation within the silicate structure should be used for the species. The alkali metal or alkaline earth cations that normally participate in the ion-exchange reactions have the ex subscript; the elements in the silicate structure use the sil subscript. The appropriate free-energy data are tabulated by Tardy and Garrels.[19] Table A-XI lists values of ΔG°_f calculated for a number of zeolite minerals by this method in the column labeled "TG." For analcime, wairakite, and laumonite, these estimates are ~10 to 20 kcal/mole more negative than the experimental results (see Table A-XI). It was observed that if $[Na_2O]_{sil}$ was used in place of $[Na_2O]_{ex}$ in Eq. (9), the estimated value of ΔG°_f was closer to the experimental result. The same was true for the other two zeolites with experimental data available. Table A-XI also lists values of ΔG°_f calculated using only free-energy data associated with the silicate structure; these results are in the column labeled "Modified TG." Although I have no justification for this modification, it produces better estimates for the three zeolites for which comparisons can be made.

Tardy and Garrels tabulated values of ΔG°_f for aqueous species;[19] these values are shown in Table A-X. They were used to convert ΔG°_f to ΔG°_r for these minerals. Table A-XII shows values of ΔG°_r and $\log_{10} K$ for these minerals calculated by the modified Tardy and Garrels method.

B. Nriagu

Nriagu proposed another simple method for estimating ΔG°_f of clay minerals.[18] He also writes a reaction for the formation of the mineral, but uses hydroxides of the elements involved. For analcime,

$$NaOH + Al(OH)_3 + 2Si(OH)_4 = NaAlSi_2O_6 \cdot H_2O + 5H_2O \quad . \tag{10}$$

The value of ΔG°_f for analcime is calculated as

$$\begin{aligned} \Delta G^{\circ}_f \text{ (analcime)} &= \Delta G^{\circ}_f(NaOH) + \Delta G^{\circ}_f(Al(OH)_3) \\ &+ 2\Delta G^{\circ}_f(Si(OH)_4) - 5\,[\Delta G^{\circ}_f(H_2O) + \sigma] \quad . \end{aligned} \tag{11}$$

The parameter σ is an empirical correction factor given the value 0.39 kcal/mole. Appropriate values of ΔG°_f for the hydroxides are tabulated by Nriagu. Table A-XI lists values of ΔG°_f for the zeolites considered in the column labeled "Nriagu." For analcime, wairakite, and laumonite, the estimated values are ~3 to 10 kcal/mole more positive than the experimental data. No attempt was made to modify this method.

Nriagu did not tabulate values of ΔG°_f for aqueous species. Data from SUPCRT[10] (see Table A-X) were used to convert ΔG°_f to ΔG°_r for this method. The results are listed in Table A-XII.

C. Chen

Chen has proposed a somewhat more complex method of estimating ΔG°_f of silicate minerals.[4] Whereas the methods of Tardy and Garrels and Nriagu have only been applied to layer silicates or clays, Chen's method has been used for a wider range of silicate minerals, including feldspar and analcime. For this

TABLE A-XI

THERMODYNAMIC DATA FOR ZEOLITES

Mineral	ΔG°_f (kcal/mole) TG[a] (Ref. 19)	Modified TG (Ref. 19)	Nriagu (Ref. 18)	Chen (Ref. 4)	Experimental ΔG°_f (kcal/mole) SUPCRT (Ref. 10)	Robie and Waldbaum (Ref. 11)
Analcime						
$Na[AlSi_2O_6]\cdot H_2O$	-747.3	-741.0	-732.5	-734.9	-738.1	-734.3
Wairakite						
$Ca[Al_2Si_4O_{12}]\cdot 2H_2O$	-1502.0	-1479.0	-1474.0	-1477.8	-1477.7	-
Laumonite						
$Ca[Al_2Si_4O_{12}]\cdot 4H_2O$	-1620.4	-1597.4	-1586.6	-1591.1	-1597.0	-
Clinoptilolite						
$Ca[Al_2Si_{10}O_{24}]\cdot 8H_2O$	-3084.8	-3061.8	-3047.8	-3045.8	-	-
$Mg[Al_2Si_{10}O_{24}]\cdot 8H_2O$	-3061.5	-3051.2	-3035.7	-3024.5	-	-
$Na_2[Al_2Si_{10}O_{24}]\cdot 8H_2O$	-3077.4	-3064.8	-3038.8	-3040.2	-	-
$K_2[Al_2Si_{10}O_{24}]\cdot 8H_2O$	-3090.0	-3090.0	-3062.8	-3065.8	-	-
Heulandite						
$Ca[Al_2Si_7O_{18}]\cdot 6H_2O$	-2352.6	-2329.6	-2317.2	-2318.4	-	-
Mordenite						
$Na[AlSi_5O_{12}]\cdot 3H_2O$	-1479.5	-1473.2	-1463.1	-1463.2	-	-
$K[AlSi_5O_{12}]\cdot 3H_2O$	-1485.8	-1485.8	-1475.1	-1476.2	-	-

[a]Tardy and Garrels.

TABLE A-XII

THERMODYNAMIC DATA FOR ZEOLITES

Mineral	ΔG°_r (kcal/mole)			$\log_{10} K$			Experimental $\log_{10} K$	
	Modified TG[a] (Ref. 19)	Nriagu[b] (Ref. 18)	Chen (Ref. 4)	Modified TG[a] (Ref. 19)	Nriagu[b] (Ref. 18)	Chen (Ref. 4)	SUPCRT (Ref. 10)	WATEQF (Ref. 14)
Analcime								
$Na[AlSi_2O_6]\cdot H_2O$	+9.3	+15.5	+12.1	-6.8	-11.4	-8.8	-7.28	-9.35
Wairakite								
$Ca[Al_2Si_4O_{12}]\cdot 2H_2O$	+28.8	+29.0	+23.2	-21.1	-21.3	-17.0	-18.56	-17.40
Laumonite								
$Ca[Al_2Si_4O_{12}]\cdot 4H_2O$	+23.8	+29.8	+23.3	-17.4	-21.8	-17.1	-14.15	-13.06
Clinoptilolite								
$Ca[Al_2Si_{10}O_{24}]\cdot 8H_2O$	-19.1	-9.5	-9.5	+14.0	+7.0	+7.0	-	-
$Mg[Al_2Si_{10}O_{24}]\cdot 8H_2O$	-31.8	-20.9	-11.5	+23.3	+15.3	+8.4	-	-
$Na_2[Al_2Si_{10}O_{24}]\cdot 8H_2O$	-29.3	-7.4	-11.0	+21.5	+5.5	+8.1	-	-
$K_2[Al_2Si_{10}O_{24}]\cdot 8H_2O$	-44.1	-21.5	-26.3	+32.3	+15.8	+19.3	-	-
Heulandite								
$Ca[Al_2Si_7O_{18}]\cdot 6H_2O$	+2.3	+10.1	+6.9	-1.7	-7.4	-5.1	-	-
Mordenite								
$Na[AlSi_5O_{12}]\cdot 3H_2O$	-12.2	-4.1	-5.3	+8.9	+3.0	+3.9	-	-
$K[AlSi_5O_{12}]\cdot 3H_2O$	-19.6	-11.2	-13.2	+14.3	+8.2	+9.6	-	-

[a]Tardy and Garrels.
[b]Use aqueous data from SUPCRT (Ref. 10).

method, a series of reactions forming the mineral of interest from simpler compounds is written. For analcime, three of the reactions used were

$$\frac{1}{2}\,Na_2O + \frac{1}{2}\,Al_2O_3 + 2SiO_2 + H_2O = NaAlSi_2O_6 \cdot H_2O \quad , \tag{12}$$

$$\frac{1}{2}\,Na_2SiO_3 + \frac{1}{2}\,Al_2SiO_5 + SiO_2 + H_2O = NaAlSi_2O_6 \cdot H_2O \quad , \text{ and} \tag{13}$$

$$NaAlSiO_4 + SiO_2 + H_2O = NaAlSi_2O_6 \cdot H_2O \quad . \tag{14}$$

Using standard values of ΔG°_f for the reactants, a value of ΔG°_f for analcime is calculated for each equation. Chen used ΔG°_f data from the tabulation of Robie and Waldbaum[11] in his analysis; those data were also used here. The values of ΔG°_f for the mineral of interest (analcime in this example) will differ for the various reactions. Chen observed that they tend to become more negative as the reactants become more complex, and that they seem to approach a limit. He proposed finding the limit by fitting data to the equation,

$$y_i = a \exp(bx_i) + c \quad , \tag{15}$$

where y_i is the value of ΔG°_f for the $i^{\underline{th}}$ equation and $x_i = i$ when the y_i are written in order so that $y_0 > y_1 > y_2 \ldots > y_n$. The parameter c is the limit and is taken as ΔG°_f for the mineral. Table A-XI lists values of ΔG°_f for the zeolites considered in the column labeled "Chen." For analcime, wairakite, and laumonite, the estimates are ~0 to 6 kcal/mole more positive than the experimental data.

For calculations by this method, values of ΔG°_f for aqueous species were also taken from the tabulation of Robie and Waldbaum[11] (see Table A-X). Values of ΔG°_r and $\log_{10} K$ are listed in Table A-XII.

D. Effect of Composition

Two additional calculations were done to estimate the effect of changing the Si/Al ratio and the amount of water of hydration. The calculations were done for Ca-clinoptilolite ($Ca[Al_2Si_{10}O_{24}] \cdot 8H_2O$) only; it has a Si/Al ratio of 5 and has 8 molecules of water of hydration as the formula is written. Table A-XIII shows values of ΔG°_f and $\log_{10} K$ for Si/Al ratios of 3, 4, and 5. These minerals become less stable ($\log_{10} K$ becomes more negative) as the Si/Al ratio is reduced. Table A-XIV shows values of ΔG°_f and $\log_{10} K$ as the number of molecules of water of hydration varies from 4 to 10. Chen's method predicts no effect for $\log_{10} K$, but the modified Tardy and Garrels' method and Nriagu's method predict opposite effects.

E. Discussion of Estimated Data

The estimated values of ΔG°_f for the three zeolites (clinoptilolite, heulandite, and mordenite) are in relatively good agreement. There is less than 1% difference between results from the modified Tardy and Garrels' method, Nriagu's method, and Chen's method (see Table A-XI). In most cases, Nriagu's method and Chen's method agree within 0.1%. However, in terms of $\log_{10} K$ for the aqueous reaction, large relative differences exist (see Table A-XII). The only gauges of accuracy for these estimates are the comparisons for analcime,

TABLE A-XIII

EFFECT OF Si/Al RATIO ON ΔG°_f AND $\log_{10} K$

Formula	Si/Al Ratio	ΔG°_f (kcal/mole) Modified TG (Ref. 19)	Nriagu (Ref. 18)	Chen (Ref. 4)	$\log_{10} K$ Modified TG (Ref. 19)	Nriagu (Ref. 18)	Chen (Ref. 4)
$Ca[Al_2Si_6O_{16}]\cdot 8H_2O$	3	-2243.4	-2223.8	-2227.2	-2.1	-13.0	-9.0
$Ca[Al_2Si_8O_{20}]\cdot 8H_2O$	4	-2652.6	-2635.8	-2636.5	+6.0	-3.0	-1.0
$Ca[Al_2Si_{10}O_{24}]\cdot 8H_2O$	5	-3061.8	-3047.8	-3045.8	+14.0	+7.0	+7.0

TABLE A-XIV

EFFECT OF WATER OF HYDRATION ON ΔG°_f AND $\log_{10} K$

Water of Hydration[a] n	ΔG°_f (kcal/mole) Modified TG (Ref. 19)	Nriagu (Ref. 18)	Chen (Ref. 4)	$\log_{10} K$ Modified TG (Ref. 19)	Nriagu (Ref. 18)	Chen (Ref. 4)
4	-2825.0	-2822.6	-2819.0	+6.7	+8.1	+7.0
6	-2943.4	-2935.2	-2932.4	+10.3	+7.6	+7.0
8	-3061.8	-3047.8	-3045.8	+14.0	+7.0	+7.0
10	-3180.2	-3160.4	-3159.2	+17.7	+6.4	+7.0

[a]n is defined in $Ca[Al_2Si_{10}O_{24}]\cdot nH_2O$.

wairakite, and laumonite. Even these comparisons may not carry much weight because the Si/Al ratio and water of hydration of clinoptilolite, heulandite, and mordenite are generally quite different than for analcime, wairakite, and laumonite. Any inherent errors in the methods that are associated with these variables could lead to inaccurate estimates.

Another problem with these methods is that they estimate the same free energy for polymorphs. Wairakite and laumonite have different structures, as well as having a different number of waters of hydration.[5] The only difference in the ΔG°_f or $\log_{10}$ K estimates, however, is from the water of hydration. The difference in the experimental values of $\log_{10}$ K of wairakite and laumonite is ~4; Chen's method shows no difference in the estimates of the two values and Nriagu's method shows only ~0.5. Another method of estimating ΔG°_f, developed by Slaughter, can account for the structure of the mineral, but at the expense of considerable complexity in the calculations.[21-23]

V. SUMMARY AND CONCLUSIONS

A preliminary search has been conducted for free-energy data at 25°C for some of the mineral phases found during exploratory drilling at or near Yucca Mountain. Data were found for silica (quartz, cristobalite, and amorphous silica), alkali feldspars, some clays, and one zeolite (analcime). Data were estimated for three other zeolites (clinoptilolite, heulandite, and mordenite).

When data are available from the SUPCRT compilation,[10] I think that they should be used because it provides a reliable and internally consistent data set. However, there were no data for any clays of interest in SUPCRT and only for one zeolite. Being forced to resort to estimation techniques to obtain data for three zeolites adds additional uncertainty to those data. Differences in $\log_{10}$ K for aqueous reactions among the three estimation methods are relatively large (see Table A-XII). I would choose the data estimated by Chen's method[4] for use in modeling calculations because I think his method is more generally applicable than the others. However, I think that a review of the estimated data points out the need for experimental thermodynamic data for

these minerals if the results of modeling calculations are to be accurate. This need also holds for the clays. Although thermodynamic data are available for some clay minerals, the Yucca Mountain clays do not match the composition of these materials.

This review has concentrated on thermodynamic data at 25°C. Many of the sources used here have higher temperature data, too. In principle, Chen's method could also be used to estimate higher temperature data as long as values of ΔG°_{f} were available for simpler compounds at the temperature of interest. The other two methods could not easily be employed at other temperatures because they depend on specific data sets that were prepared by the authors for 25°C only. Thus, thermodynamic data sets could also be prepared at temperatures other than 25°C.

Although the data generated in this review are not adequate for accurate chemical-equilibrium calculations, they can be used to learn how to model the Yucca Mountain groundwater system, what modeling codes are most appropriate, and where further effort is needed in areas other than the chemical-equilibrium calculations. Results from equilibrium calculations can be compared with groundwater analyses. These comparisons can test the accuracy of the thermodynamic data, but they also test assumptions about the minerals, the groundwater, and how they interact. It may be difficult to uncover the cause of any discrepancies if both thermodynamic data and model assumptions are suspect.

REFERENCES

1. G. H. Heiken and M. L. Bevier, "Petrology of Tuff Units from the J-13 Drill Site, Jackass Flats, Nevada," Los Alamos Scientific Laboratory report LA-7563-MS (February 1979).

2. M. L. Sykes, G. H. Heiken, and J. R. Smyth, "Mineralogy and Petrology of Tuff Units from the UE25a-1 Drill Site, Yucca Mountain, Nevada," Los Alamos Scientific Laboratory report LA-8139-MS (November 1979).

3. A. C. Walters and P. R. Carroll, Eds., "Preliminary Stratigraphic and Petrologic Characterization of Core Samples from USW-G1, Yucca Mountain, Nevada," Los Alamos National Laboratory report LA-8840-MS (November 1982).

4. C. H. Chen, "A Method of Estimation of Standard Free Energies of Formation of Silicate Minerals at 298.15 K," Am. J. Sci. 275, 801-817 (1975).

5. W. A. Deer, R. A. Howie, and J. Zussman, Rock-Forming Minerals, Vol 3, Sheet Silicates (Longman Group Ltd., London, 1962), pp. 191-245.

6. H. C. Helgeson, "Thermodynamics of Hydrothermal Systems at Elevated Temperatures and Pressures," Am. J. Sci. 267, 729-804 (1969).

7. J. R. Smyth and A. Caporuscio, "Review of the Thermal Stability and Cation Exchange Properties of the Zeolite Minerals Clinoptilolite, Mordenite, and Analcime: Applications to Radioactive Waste Isolation in Silicic Tuff," Los Alamos National Laboratory report LA-8841-MS (June 1981).

8. J. R. Boles, E. M. Flanigen, A. J. Gude, R. L. Hay, F. A. Mumpton, and R. C. Surdam, "Mineralogy and Geology of Natural Zeolites," in Mineralogical Society of America Short Course Notes, Vol. 4, F. A. Mumpton, Ed. (Southern Printing Co., Blacksburg, Virginia, 1978).

9. W. A. Deer, R. A. Howie, and J. Zussman, Rock-Forming Minerals, Vol. 4, Framework Silicates (Longman, Green and Company, Ltd., London, 1963), pp. 351-428.

10. H. C. Helgeson, J. M. Delany, H. W. Nesbitt, and D. K. Bird, "Summary and Critique of the Thermodynamic Properties of Rock-Forming Minerals," Am. J. Sci. 278A, 1-299 (1978).

11. R. A. Robie and D. R. Waldbaum, "Thermodynamic Properties of Minerals and Related Substances at 298.15°K (25.0°C) and One Atmosphere (1.013 Bars) Pressure and at Higher Temperatures," US Geological Survey Bulletin 1259 (1968).

12. L. V. Benson and L. S. Teague, "A Tabulation of Thermodynamic Data for Chemical Reactions Involving 58 Elements Common to Radioactive Waste Package Systems," Lawrence Berkeley Laboratory report LBL-11448 (August 1980).

13. T. J. Wolery, "Calculation of Chemical Equilibrium Between Aqueous Solution and Minerals: The EQ3/6 Software Package," Lawrence Livermore Laboratory report UCRL-52658 (February 1979).

14. L. N. Plummer, B. F. Jones, and A. H. Truesdell, "WATEQF: A FORTRAN IV Version of WATEQ, A Computer Program for Calculating Chemical Equilibrium of Natural Waters, Users Guide," US Geological Survey report USGS-WRI-76-13 (September 1976).

15. G. Sposito and S. V. Mattigod, "GEOCHEM: A Computer Program for the Calculation of Chemical Equilibria in Soil Solutions and Other Natural Water Systems," Department of Soil and Environmental Sciences, University of California, Riverside, California (1979).

16. S. E. Ingle, M. D. Schuldt, and D. W. Schults, "A User's Guide for REDEQL.EPAK," Environmental Protection Agency report EPA-600/3-78-024 (February 1978); S. E. Ingle, J. A. Keniston, and D. W. Schults, "REDEQL.EPAK, Aqueous Chemical Equilibrium Program," Corvallis Environmental Research Laboratory, Corvallis, Oregon (1979).

17. J. W. Ball, D. K. Nordstrom, and E. A. Jenne, "Additional and Revised Thermochemical Data and Computer Code for WATEQ2 - A Computerized Chemical Model for Trace and Major Element Speciation and Mineral Equilibria of Natural Waters," US Geological Survey Water Resources Investigations report WRI 78-116 (January 1980).

18. J. O. Nriagu, "Thermochemical Approximations for Clay Minerals," Am. Mineral. 60, 834-839 (1975).

19. Y. Tardy and R. M. Garrels, "A Method of Estimating the Gibbs Energies of Formation of Layer Silicates," Geochim. Cosmochim. Acta 38, 1101-1116 (1974).

20. S. V. Mattigod and G. Sposito, "Improved Method for Estimating the Standard Free Energies of Formation (ΔG°_f, 298.15) of Smectites," Geochim. Cosmochim. Acta 42, 1753-1762 (1978).

21. M. Slaughter, "Chemical Binding in Silicate Minerals-I. Model for Determining Crystal-Chemical Properties," Geochim. Cosmochim. Acta 30, 299-313 (1966).

22. M. Slaughter, "Chemical Binding in Silicate Minerals-II. Computational Methods and Approximations for the Binding Energy of Complex Silicates," Geochim. Cosmochim. Acta 30, 315-322 (1966).

23. M. Slaughter, "Chemical Binding in Silicate Minerals-III. Application of Energy Calculations to the Prediction of Silicate Mineral Stability," Geochim. Cosmochim. Acta 30, 323-339 (1966).

☆U.S. GOVERNMENT PRINTING OFFICE: 1982-0-576-020/80